Research Square

Preprints are preliminary reports that have not undergone peer review.
They should not be considered conclusive, used to inform clinical practice,
or referenced by the media as validated information.

An exploratory study of the physicochemical, thermal, structural, and spectroscopic properties of agricultural residue composite briquettes for domestic energy applications

Umaru Ahmadu
Federal University of Technology
Yakubu Bala Alhaji
Federal Polytechnic Bida
Halilu Ibrahim Jume
Federal University of Technology
Abubakar Sadiq Yusuf
sadiq.yusuf@vuw.ac.nz
Victoria University of Wellington
Moses Agida
Federal University of Technology
Bello Abdulkadir
Federal University of Technology

Research Article

Keywords: Biomass briquettes, Rice husk, Palm kernel shell, Groundnut shell, physicochemical characterisation, Thermal analysis, Solid fuel

Posted Date: November 19th, 2026

DOI: https://doi.org/10.21203/rs.3.rs-11419465/v1

License: This work is licensed under a Creative Commons Attribution 4.0 International License.
Read Full License

Additional Declarations: No competing interests reported.

An exploratory study of the physicochemical, thermal, structural, and spectroscopic properties of agricultural residue composite briquettes for domestic energy applications

U. Ahmadu[1]*, B. Y. Alhaji[1, 2], H.I. Jume[1], A. S., Yusuf [1, 3,5], M. Agida[1], B. Abdulkadir[4]

[1] School of Physical Sciences, Department of Physics, Federal University of Technology, PMB 65, Minna, Niger State, Nigeria.*

[2]Department of Physics, Federal Polytechnic Bida, Nigeria.

[3]School of Engineering, Computer and Mathematical Sciences, Auckland University of Technology, PO Box 92006, Auckland 1142, New Zealand.

[4]Department of Mechanical Engineering, Federal University of Technology, Minna, Nigeria.

[5]Robinson Research Institute, Victoria University of Wellington, PO Box 33436, Petone 5046, New Zealand

[*]Corresponding authors: umaruahmadu@futminna.edu.ng, sadiq.yusuf@vuw.ac.nz

ABSTRACT

Over 600 million people in Africa lack clean cooking fuels and electricity, leading to heavy reliance on firewood and charcoal, deforestation, and environmental pollution from open burning. Agricultural residues such as rice husk (RH), palm kernel shell (PKS), and groundnut shell (GS) are abundant in Nigeria but remain underutilized as solid biofuels. While single-biomass briquettes have been studied, the synergistic effects of blending these complementary feedstocks into binary and ternary composite briquettes require thorough characterization. This study evaluated the production and comprehensive physicochemical, thermal, and structural characterization of eight briquette formulations, comprising three pure, two binary, and three ternary blends of RH, PKS, and GS using 10% cassava starch as a binder to identify optimal biofuel composites for domestic heating and cooking applications. Characterization involved proximate and ultimate analyses, bomb calorimetry (HHV/LHV), lignocellulosic compositional analysis, TGA/DTG, DSC, XRD, SEM/EDX, and FTIR. Moisture content across all samples remained under 10%, with composite briquettes exhibiting lower moisture and higher volatile matter (74.46–86.48%) than pure biomass (56.22–70.21%), facilitating higher ignitability. Ash content scaled with RH proportion, reaching a maximum of 18.60% in Sample C (RH80:GS10: PKS10). PKS100 yielded the highest energy content (HHV=21.79 MJ/kg). High lignin contents in PKS100 (58.72%) and GS100 (60.26%) contributed to enhanced structural integrity and natural binding. Blend D demonstrated optimal overall properties with high volatile matter (86.48%), low moisture (5.24%), moderate ash (7.48%), and superior thermal buffering confirmed via DSC. TGA/DTG showed that high-RH blends (Samples B and C) maintained thermal insulation up to >691 °C due to silica content. XRD

revealed predominantly amorphous to nanocrystalline structures across samples. Blend D is recommended as the optimal composite for domestic heating and cooking due to its high energy density, low moisture, and superior ignition profile, while Blend C is best suited for applications requiring high thermal durability. Utilizing these agro-waste composite briquettes presents a viable pathway to reduce firewood dependency, and advance waste-to-energy technologies in sub-Saharan Africa.

Keywords: *Biomass briquettes, Rice husk, Palm kernel shell, Groundnut shell, physicochemical characterisation, Thermal analysis, Solid fuel.*

Introduction

Energy is fundamental to economic development, and its efficient production and use are central to global sustainability. Biomass, as a renewable energy resource, occupies an increasingly important position in the world's energy mix because it can be produced locally, offsets dependence on fossil fuels, and is generally regarded as carbon-neutral: the carbon dioxide released on combustion is broadly offset by the carbon dioxide absorbed during plant growth (Danso-Boateng & Achaw, 2022). Concerns over climate change, the drive to cut greenhouse gas emissions, and volatile fossil-fuel prices have together strengthened the case for expanding biomass utilisation as part of a diversified and sustainable energy supply.

Biomass refers to organic matter derived from plant and animal material, composed mainly of cellulose, hemicellulose, lignin, and other organic constituents such as resins and starches. It can be converted into solid, liquid, and gaseous fuels through thermochemical routes: combustion, pyrolysis, gasification, torrefaction, and carbonization; or through biochemical routes such as anaerobic digestion, fermentation, and transesterification, yielding products ranging from charcoal and briquettes to bio-ethanol, biogas, and syngas (Danso-Boateng & Achaw, 2022). No single pre-treatment or conversion route suits every feedstock; the most appropriate choice depends on the nature of the biomass, whether woody, agricultural, or herbaceous.

Nigeria generates substantial quantities of agricultural residue, including rice husk, groundnut shell, and palm kernel shell, alongside forest and livestock waste, giving the country an agricultural-residue energy potential estimated at roughly 1.09 EJ (Jekayinfa, Orisaleye, & Pecenka, 2020). In practice, most of this resource remains untapped in rural areas, where residues are typically disposed of by open burning or left to decompose on farmland rather than converted into useful energy (Jekayinfa et al., 2020). This practice is both an environmental hazard and a lost economic opportunity. In their raw state, these residuesit also poorly suited for direct use as fuel

because they are bulky, have low bulk density, high moisture content, and inconsistent particle size and shape, all of which make them difficult to store, transport, and burn efficiently (Ibitoye, Jen, Mahamood, & Akinlabi, 2021).

Pre-treatment of biomass before combustion can address many of these shortcomings using techniques such as drying, grinding, sieving, briquetting, and carbonization alter the physical and chemical structure of raw biomass, increasing its bulk density, calorific value, and combustion efficiency while making it easier to store and transport (Ibitoye et al., 2021). Briquetting, i.e., compacting loose biomass particles under pressure, with or without a binder, into a densified solid fuel has been demonstrated within Nigeria and outside using precisely the residues of interest to this project, rice husk, groundnut shell, and palm kernel shell (Emmanuel, Adamu, Rumba, & Hussaini, 2023; Jume et al., 2024; Bonsu, Takase, & Mantey, 2020). Taken together, the poor utilization of Nigeria's abundant agricultural residues, the inefficiency and health burden of traditional cookstoves, and the demonstrated potential of briquetting and carbonization to convert these residues into a clean, dense, and transportable solid fuel form the rationale for this study.

The present study integrates physicochemical, thermal, and structural characterization within a single analytical framework. This approach provides a comprehensive understanding of the relationships between biomass composition, thermal degradation, structural evolution, and combustion performance and offers a stronger scientific basis for briquette optimization than reliance on individual analytical techniques.

Materials and methods

The materials, preparation procedures, briquette production process, and analytical methods used in this study are described in this section. The methods are presented in the recommended sequence for solid biofuel characterization: raw material and feedstock preparation, proximate analysis, ultimate analysis, calorific value determination, lignocellulosic compositional analysis, and advanced thermal and structural characterization (TGA/DTG, DSC, XRD, SEM, FTIR, and EDX).

Materials

Rice husk (RH), groundnut shell (GS), palm kernel shell (PKS), and cassava starch (CS) were used as biomass feedstocks in this study. These agricultural residues were selected due to their abundance in north-central Nigeria, their potential as solid biofuels, and to evaluate their individual and blended characteristics during briquetting.

Material preparations and briquette formulation

Raw biomass feedstocks, rice husk, groundnut shell, and palm kernel shell were obtained from Etsu Yahaya Oil Mill in Bida (located 3 km along Minna Road) and Kontagora Rice and Groundnut Mills along Rijau Road, Kontagora, Niger State, Nigeria. All collected raw materials were transported to the NRF2021 Laboratory (Biomass Briquetting and Cookstove Testing), Department of Physics, Federal University of Technology Minna (FUT Minna), Nigeria, for further processing.

Impurities such as stones, dust, metal debris and extraneous plant matter were manually removed. The cleaned biomass raw materials were sun-dried for 48 h to remove surface moisture.

The dried and purified raw materials were reduced in particle size using a 5-hp electrical grinding machine at the Central Workshop, Department of Mechanical Engineering, FUT Minna. 100 kg quantity of each material was manually fed into the hopper and subjected to repeated pulverization: two passes over 2 h for rice husk; three passes over 3 h for groundnut shells; and four passes over 4 h for palm kernel shells, until a target particle size of 1.5 mm was achieved. The pulverized materials were then sun-dried for 72 h at ambient temperature to remove residual moisture absorbed from external sources. The biomass powder samples were subsequently sieved to obtain a uniform 1 mm particle size. The dried samples were sealed and stored in low-humidity polyethylene sacks until required for densification.

Cassava starch, purchased from Mokwanla Market, Bida Local Government Area, Niger State, was used as a natural binding agent. The preparation of the cassava starch gel was conducted at the NRF2021 Laboratory, Department of Physics, FUT Minna. 500 g of dry cassava starch was mixed uniformly with 1 L of cold water. Separately, 3 L of cold water was measured into a 600 g capacity aluminum pot and heated on a charcoal stove (following a 10-minute pre-ignition phase) fueled by 10 mL of kerosene. After heating the water to approximately 60–70°C (over approximately 15 minutes, prior to boiling), the prepared starch slurry was poured into the warm

water and continuously stirred until a homogeneous gel was formed upon reaching the boiling point. To prevent premature coagulation or agglomeration of undissolved starch granules, care was taken not to let the water boil prior to adding the starch mixture. The resulting cassava starch gel was allowed to cool to room temperature over 3 h before application.

The pulverized biomass samples were mixed with 10% (w/w) cassava starch gel binder across six formulation groups: pure (pristine), binary and ternary samples. All formulations were mixed manually in clean 50 L plastic containers. The mass mixing ratios are summarized in Table 1.

Table 1

Blending ratios of biomass samples with 10% cassava starch gel binder.

SAMPLES ID	MASS BY RATIO (wet %)	CLASSIFICATION OF SINGLE/BLENDS
A	RH40:GS30: PKS30	Ternary
B	RH60:GS20: PKS20	Ternary
C	RH80:GS10: PKS10	Ternary
D	GS50:PKS50	Binary
E	RH50:GS50	Binary
F	RH100	Pristine
G	GS100	Pristine
H	PKS100	Pristine

Briquettes were produced in the NRF2021 Laboratory using a manually operated hydraulic piston briquetting press. Blended biomass were introduced into cylindrical steel moulds having an internal diameter of 50.00 mm, an external diameter of 70.00 mm, and a central hole of 15.0 mm outer diameter to form an axial hole in each briquette. The central longitudinal hole increases briquette porosity, improving air ventilation during combustion and enhancing burning efficiency. Densification was performed at 30°C under a hydraulic pressure of 120 bar. A dwell time of 5 min was applied to each charge to mitigate elastic recovery (spring-back) after ejection from the mould. Twelve (12) briquettes were produced per formulation, and their immediate wet masses were recorded. The produced briquettes were placed on a flat surface and sun-dried in a well-ventilated outdoor environment for 31 days until reaching a constant mass prior to characterization.

Combustion properties

The moisture content (MC), volatile matter (VM), ash content (AC), and fixed carbon (FC) of each sample were determined in accordance with standard methodologies. All ground samples possessed a particle size of ≤1 mm, achieved using standard test sieves as per ASTM D2013-86. ASTMs and other standards were all modified somewhat to suit the situation, which was basically taking measurements once only, and should therefore be considered exploratory at this stage.

Moisture Content

A 1.0 g sample of powdered biomass was placed in a pre-weighed aluminum dish and dried in an oven at 105°C for 1 h. The dish was then cooled in a desiccator and re-weighed according to ASTM D2444-16. Moisture content was calculated using Equation (1):

$$\textit{Moisture Content (\%MC)} = \frac{W_1 - W_3}{W_2 - W_1} \times 100\ \% \qquad (1),$$

where, W_1 is the weight of the empty dish, W_2 is the weight of the dish and sample prior to oven drying, and W_3 is the weight of the dish and sample after oven drying.

Volatile Matter

A 1.0 g sample was weighed into a pre-weighed, lidded crucible and combusted in a muffle furnace according to ASTM D3175-18 for particulate wood fuels. The sample was held at 105°C and subsequently heated to 950°C for 7 min. The crucible was then removed, cooled in a desiccator, and re-weighed. Volatile matter content was calculated using Equation (2):

$$\textit{Volatile Matter (\%VM)} = \frac{W_2 - W_3}{W_2} \times 100\ \% \qquad (2),$$

where W_2 is the sample mass after drying at 105∘C, and W_3 is the sample mass remaining after heating at 950∘C.

Ash Content

Ash content was determined according to ASTM D3174-12. A 1.0 g sample was placed into a pre-weighed crucible and ignited in a muffle furnace at 760∘C until complete ash formation (white or light grey residue) was observed. After cooling in a desiccator, ash content was calculated using Equation (3):

$$\textit{Ash Content (\%)} = \frac{W_3 - W_2}{W_2 - W_1} \times 100\ \% \qquad (3)$$

where W_1 is the weight of the empty crucible, W_2 is the weight of the crucible and sample prior to incineration, and W_3 is the weight of the crucible and ash residue following combustion.

Fixed carbon

The percentage of fixed carbon was calculated by difference using Equation (4):

$$Fixed\ Carbon\ (\%FC) = 100 - (\%MC + \%VM + \%AC) \quad (4)$$

Ultimate analysis (elemental composition)

The elemental composition (C, H, N, S, and O) of powdered briquette samples was measured using a HACH Model DR/2010 LE 811 Series CHNSO elemental analyzer. Test specimens (3–4 mg, particle size ≤1 mm) were encapsulated in tin foil and introduced into the analyzer's combustion chamber. Gaseous combustion products (CO_2, H_2O vapor, and N_2) were separated chromatographically and quantified using a thermal conductivity detector (TCD). Measurements were calibrated using reference standards in accordance with ASTM E777-08 and ASTM E778-08, including 2,5-bis (5-tert-butyl-2-benzoxazol-2-yl) thiophene (BBOT) and oatmeal. All measurements were performed once only since the work is exploratory. Oxygen content was determined by difference using Equation (5):

$$Oxygen\ (\%) = 100 - (\%C + \%H + \%N + \%S + \%Ash) \quad (5)$$

Calorific value determination

Composite samples A–E (bomb calorimetry)

The higher heating values (HHV) of composite samples A, B, C, D, and E were determined using an oxygen bomb calorimeter in accordance with ASTM D3176-15. A 0.5 g sample was placed in a clean crucible within the calorimeter electrode assembly. A cotton ignition thread was positioned in contact with the sample surface. The vessel was pressurized with oxygen to 3000 kPa (3.0 MPa) and allowed to stabilize for 1 min before placement into the calorimeter jacket. Automatic temperature tracking and heat measurement were logged digitally, and residual unburned wire was accounted for post-combustion.

Pure biomass samples F, G, and H

The heating values of single-biomass samples F (RH100), G (GS100), and H (PKS100) were determined according to ASTM D5865-13 using an XRY-1A oxygen bomb calorimeter at the National Centre for Energy Research and Development, University of Nigeria, Nsukka (UNN). A 10 cm length ignition wire was connected across the electrode poles in contact with the sample. The bomb cylinder was charged with 10 mL of distilled water and pressurized with oxygen gas to 2.8–3.0 MPa. Initial water temperature (T_0) was recorded after 2 min of continuous stirring, and final combustion temperature (T_f) was recorded at 31 min. Unburned wire lengths were measured, and the internal bomb washings were titrated with 0.0709 N sodium carbonate (Na_2CO_3) solution using methyl red indicator to correct for nitric and sulfuric acid formation. Higher heating value (HHV) and lower heating value (LHV) were further evaluated using the modified Dulong–Milne correlation (Sheng and Azevedo, 2005) given in Equation (6):

$$Calorific\ Value\ (MJ/kg) = -1.3675 + 0.3137C + 0.7009H + 0.0318O \quad (6)$$

Compositional analysis

The structural components (cellulose, hemicellulose, and lignin) of the biomass samples were quantified using standard sequential extraction techniques based on AOAC Method 973.18.

Acid detergent fiber and acid detergent lignin

Acid detergent fiber (ADF) was determined via filtration. A 1.0 g sample (W1) was placed in a pre-weighed fritted crucible, defatted using acetone, and boiled sequentially in an acid detergent solution (ADS) for 60 min. The residue was dried in an oven at 130°C for 2 h, cooled in a desiccator, and weighed (W_2). To determine ADL, 25 mL of 72% H_2SO_4 was added to the residue in the crucible and allowed to react for 3 h with hourly stirring. The acid was filtered out, and the sample was washed with deionized water until free of acid. The crucible was dried at 130∘C for 2 h, cooled, and weighed (W_4). The sample was then ashed at 525±15°C for 3 h, cooled, and re-weighed (W_5). The percentages of ADF, ADL, and cellulose were calculated using Equations (7) and (8):

$$\% ADF = \frac{W_2-(W_3+C)}{W1} \text{ x } 100 \quad (7)$$

$$\% ADL = \frac{W_4-(W_5+C)}{W1} \text{ x } 100 \quad (8),$$

Where W_1 is the initial sample mass, W_2 is the dry crucible and residue weight after ADS extraction, W3 is the empty crucible weight, W_4 is the crucible and residue mass post-acid treatment, W_5 is the crucible and ash residue weight post-ignition, and C is the blank correction factor.

2.8.2 Neutral detergent fiber

Neutral detergent fiber (NDF) was quantified using a filtration technique. Approximately 1.00 g of Celite filter aid was added to a pre-dried crucible (W_1), followed by 0.50 g of sample. After defatting 25 mL of acetone, the sample was rinsed with water. To prevent foaming, 50 mL of cold Neutral Detergent Solution (NDS) and 0.5 g of Na_2SO_3 were added. The mixture was refluxed for 30 min, washed thoroughly with hot deionized water, and dried in an oven at 130±2°C for 2 h. The crucible was cooled to room temperature in a desiccator and weighed (W_2). After ashing at

520±25◦C for 3 h, the crucible was cooled and weighed (W_3). NDF and hemicellulose contents were computed using Equation (9):

$$\% NDF = \frac{W_2 - W_3 + blank)}{W1} \text{ x } 100 \quad (9)$$

% Hemicellulose = %NDF−%ADF

Thermal analysis

Thermogravimetric analysis was performed using a TGA 4000 analyzer (PerkinElmer, Netherlands) equipped with an automated data acquisition system. Samples pulverized to <53 μm were heated from ambient conditions (∼55◦C) to 900◦C at a constant heating rate of 10∘C/min under a continuous nitrogen (N_2) atmosphere, with an isothermal hold at 900◦C for 10 min. DTG curves were derived from the primary TGA profiles to identify peak mass loss rate temperatures (T_{max}) corresponding to distinct stages of moisture evaporation, hemicellulose decomposition, cellulose degradation, and lignin thermal breakdown.

Differential scanning calorimetry

DSC analysis was conducted using a DuPont 2100 thermal analysis system equipped with standard calorimetric modules. Thermal transitions, including endothermic moisture volatilization, glass transition, hemicellulose softening, and exothermic oxidative breakdown were evaluated for pure and blended samples. The heating rate was 10ºC per min from 59 to 300ºC. DSC thermograms were interpreted alongside TGA/DTG data to quantify enthalpies associated with major thermal events.

X-ray diffraction analysis

Wide-angle X-ray diffraction (WAXD) profiles were collected on a Thermo Scientific ARL'XTRA X-ray diffractometer (Serial No. 197492086) utilizing Cu-Kα radiation (λ=1.54060 A˚) operated at 45 kV and 40 mA. Diffraction patterns were recorded across a 2θ range of 5◦ to 60◦ with a step size of 0.05◦ and a scan rate of 1◦C/min at room temperature. Crystalline phase identification was carried out using integrated system software. Interplanar lattice spacings (d) were calculated via Bragg's Law according to Equation (10):

$$n\lambda = 2d\sin\theta \quad (10)$$

where n is an integer order of reflection, λ is the X-ray wavelength, θ is the diffraction angle, and d is the interplanar spacing. The full width at half maximum (FWHM) of characteristic peaks was subsequently utilized to estimate average crystallite size via the Scherrer equation.

Scanning electron microscopy with energy-dispersive x-ray spectroscopy

Surface morphology was evaluated using a Phenom World SEM (Model PRO, Serial No. MVE01570775) operating at an accelerating voltage of 20 kV. Powdered specimens were mounted onto double-sided conductive adhesive carbon tabs and sputter-coated with a 5 nm gold film using a Quorum Technologies Q150R coater to eliminate surface charging. Samples were visually aligned in optical mode prior to switching to electron imaging mode. Micrographs were captured at scale magnifications corresponding to 80 μm and 100 μm. Elemental analysis (weight % and atomic %) was performed concurrently using an integrated Phenom World EDX detector to corroborate crystalline phase distributions identified by XRD.

Fourier transform infrared spectroscopy

Functional group characterization was performed via FTIR spectroscopy using a Shimadzu FTIR-8400S spectrophotometer. Powdered samples were evaluated directly using an Attenuated Total Reflectance (ATR) sample stage. Background spectrum acquisition was conducted prior to sample measurements to correct for ambient atmospheric interference. Transmittance spectra were recorded across the mid-infrared region (4000–500 cm^{-1}) at a spectral resolution of 4 cm^{-1}. Observed absorption bands were indexed against reference spectral libraries for functional group identification.

Results and discussion

Proximate analysis

The experimental results are presented in sequence according to the applied analytical methodologies. The discussion begins with basic fuel quality parameters (proximate analysis, ultimate analysis, and calorific values), moves into structural compositional analysis, and concludes with advanced thermal and microstructural characterizations.

Biomass fuels are primarily characterized by four proximate parameters: Moisture Content (MC), Volatile Matter (VM), Ash Content (AC), and Fixed Carbon (FC). These parameters serve as foundational metrics for predicting devolatilization dynamics, calorific yields, and overall combustion behavior.

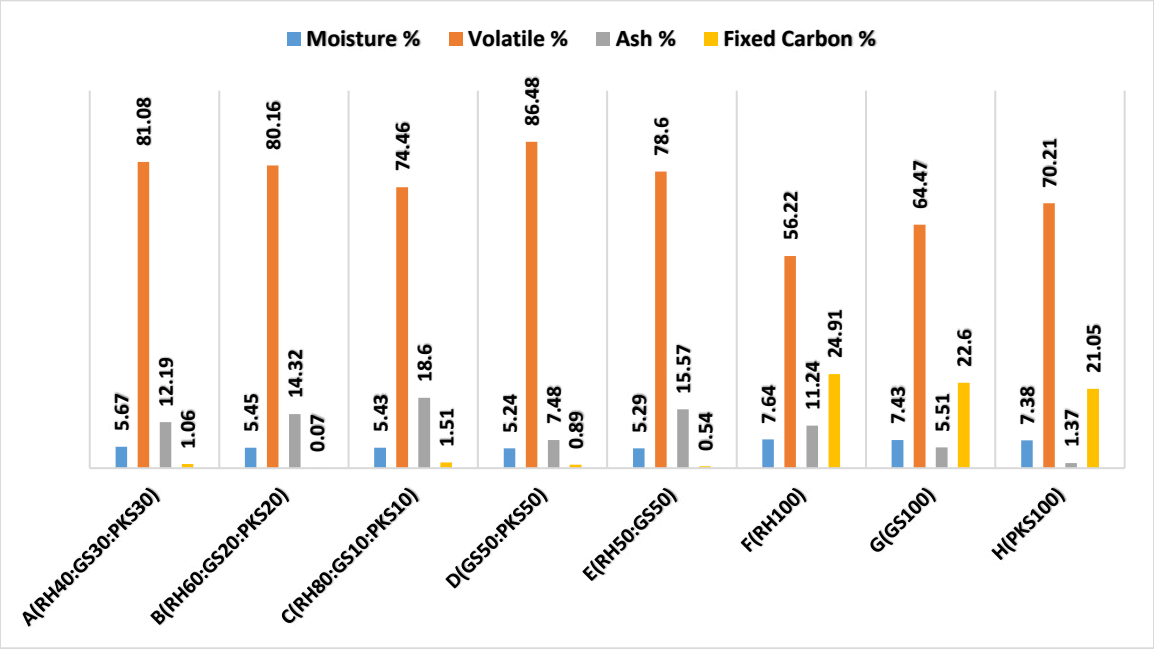


Fig. 4. The plot of proximate analysis of the composite and pure samples

Moisture content

The moisture content of raw rice husk (RH100) was observed at 7.64% (Figure 4), falling within the ranges reported in published literature. For example, (Martinez et al., 2021) observed a slightly higher value of 8.61% (dry basis), which can be attributed to differences in sun-drying conditioning protocols. The value in this study is close to the 7.0% (wet basis) reported by (El-Sayed, 2019). Conversely, (Emmanuel et al., 2023) reported a lower value of 3.96% due to pre-drying procedures prior to testing, while (Ndecky et al., 2022) and (Fauzan et al., 2018) recorded

5.88% and 9.12%, respectively. The obtained value of 7.64% reflects a standard air-dried raw rice husk, validating the adequacy of the sample preparation method used.

The moisture content for palm kernel shells (PKS100) was 7.38%, demonstrating strong agreement with published data. This value is higher than the 1.08% (wet basis) reported by (Osei Bonsu et al., 2020), which likely represented oven-dried conditions, but lower than the 10.75% reported by (Fuad et al., 2020), which was influenced by humid storage conditions. Results from (Umar et al., 2020) (6.00%) and (Acevedo et al., 2018) (7.52%) closely align with the 7.38% obtained here. PKS100 exhibited the lowest moisture content among the three individual biomasses, which is expected due to the low hygroscopicity of palm kernel shells given their dense cell architecture and elevated lignin content.

For groundnut shells (GS100), the moisture content was recorded at 7.43%. This falls between the values reported by (Emmanuel et al., 2023) (5.41%), (Perea et al., 2018) (5.79%, dry basis), and (Rathod et al., 2023) (9.5%). A significantly higher moisture content of 23.10% was reported by (Onochie et al., 2023), indicative of freshly harvested, unconditioned biomass. The 7.43% value confirms suitable air-drying across all three raw biomass types.

All composite briquettes (A–E) exhibited moisture contents ranging between 5.24% and 5.67%, representing a clear reduction compared to the pure biomass feedstock. Densification and blending physically compressed the inter-particle void spaces, thereby reducing capillary water absorption from the surrounding air. In addition, mechanical shearing during mixing likely desorbed loosely bound surface water. Among the ternary composites, moisture affinity decreased with increasing RH fraction: sample A (RH40:GS30: PKS30) at 5.67%, sample B (RH60:GS20: PKS20) at 5.45%, and sample C (RH80:GS10:PKS10) at 5.43%. The lowest moisture content was recorded in binary sample D (GS50:PKS50) at 5.24%, where the hydrophobic lignin matrix of PKS minimized water retention. Binary sample E (RH50:GS50) registered 5.29%. All composite formulations remained well below the 10% threshold recommended for commercial solid fuel briquettes to prevent latent energy losses during ignition.

Overall, the moisture contents of all briquette formulations were within the acceptable range for commercial solid biofuels, indicating adequate drying and favourable storage stability. Low moisture content is desirable because it minimizes the energy required for water evaporation during combustion, thereby improving ignition, flame temperature, and overall thermal efficiency.

The results confirm that the drying process adopted during briquette production was effective in producing fuels suitable for domestic heating and cooking applications.

Volatile Matter

Volatile matter indicates the portion of fuel that volatilizes during thermal breakdown, directly controlling ignition speed and flame stability.

RH100 yielded a volatile matter fraction of 56.22%, which is lower than values reported in literature, such as 72.69% (Martinez et al., 2021), 80.66% (Arranz et al., 2021), 68.12% (El-Sayed, 2019), 69.74% (Emmanuel et al., 2023), 63.92% (Ndecky et al., 2022), and 61.90% (Fauzan et al., 2018). This relatively low VM content is tied to the high ash content of the sample (11.24% AC). The high silica content inherent to rice husk acts as an inorganic dilution factor, suppressing the proportion of evolving volatile organic compounds (VOCs). Thermally, lower VM yields a more sustained, char-dominated combustion profile with extended residence times in the bed.

PKS100 produced a VM of 70.21%, aligning closely with reported literature: 71.80% (Osei Bonsu et al., 2020), 75.81% (Fuad et al., 2020), 73.40% (Umar et al., 2020), 69.35% (Acevedo et al., 2018), and 67.52% (Alonge and Obayopo, 2023). The broad thermal degradation profile of PKS lignin yields a substantial fraction of condensable and non-condensable volatile gases, confirming its suitability for gaseous flame propagation.

GS100 yielded a VM of 64.47%, which is slightly lower than values reported by [Emmanuel et al., 2023] (74.26%), (Perea et al., 2018) (84.90%), and (Rathod et al., 2023) (74.60%), but comparable to (Onochie et al., 2023) (67.23%). Discrepancies are attributable to cultivar variations, soil chemistry, and regional agricultural processing methods.

Notably, all composite samples exhibited higher volatile matter yields than the pure feedstocks. Binary sample D (GS50:PKS50) recorded the highest VM at 86.48%, followed by sample A (81.08%), sample B (80.16%), sample E (78.60%), and sample C (74.46%). Combining different biomass types creates a more porous, synergistic volatile-release network during thermal degradation. In sample D, the absence of high-silica rice husk allowed full volatilization of the organic fraction of both PKS and GS. Furthermore, as the RH fraction increased across the ternary series (sample A → sample B → sample C), VM dropped systematically (81.08% → 80.16% →

74.46%), proving that the inorganic silica skeleton of RH acts as a thermal barrier that dilutes volatile evolution.

In summary, volatile matter constituted the largest combustible fraction in all briquette formulations, reflecting the lignocellulosic nature of the feedstocks. Therefore, briquettes containing higher proportions of rice husk exhibited relatively higher volatile matter, resulting in improved ignition characteristics and rapid flame propagation. Conversely, palm kernel shell-rich briquettes contained comparatively lower volatile matter but higher fixed carbon contents, leading to slower but more sustained combustion. Groundnut shell exhibited intermediate behaviour and contributed to balancing the combustion characteristics of the composite briquettes. These observations demonstrate that biomass blending effectively combines the rapid ignition properties of rice husk with the prolonged heat release associated with palm kernel shell.

Ash content

Ash content represents the non-combustible inorganic residue remaining after complete oxidation. High ash contents reduce heating efficiency and increase equipment fouling.

RH100 exhibited an ash content of 11.24% which aligns with the silica-rich nature of rice husks and is comparable to the 9.68% reported by (Arranz et al., 2021) and 12.19% by (El-Sayed, 2019). Higher values were reported by (Martinez et al., 2021) (22.37%) and (Ndecky et al., 2022) (22.90%), whereas lower values were noted by (Emmanuel et al., 2023) (6.10%) due to husk washing or pre-treatment. XRD analysis confirmed that this inorganic fraction is rich in crystalline Cristobalite and Silvialite phases.

PKS100 demonstrated an ash content of 1.37%, confirming a clean-burning organic profile. Literature reports range from 0.06% (Osei Bonsu et al., 2020) and 2.67% (Acevedo et al., 2018) up to 3.79% (Fuad et al., 2020), 5.80% (Umar et al., 2020), and 8.11% (Alonge and Obayopo, 2023). SEM imaging of PKS100 confirmed a smooth, non-agglomerated surface morphology, while XRD showed predominant organic graphite structures.

GS100 yielded an intermediate ash content of 5.51%, falling within literature ranges: 4.12% (Rathod et al., 2023), 4.26% (Perea et al., 2018), 9.32% (Emmanuel et al., 2023), and 9.48% (Onochie et al., 2023). XRD identified a distinct mineral phase, Mellite ($Ca_8Al_6MgSi_5O_{28}$), unique to the groundnut shell ash residue.

On the other hand, composite ash contents were governed by the blending ratios. Ash increased proportionally with RH addition: sample C (RH80:GS10: PKS10) reached 18.60% AC due to its high silica concentration. In contrast, binary sample D (GS50:PKS50) registered 7.48% AC, and sample E (RH50:GS50) registered 15.57%. Excessive RH fractions (as in sample C) pose operational risks regarding clinker formation, slagging, and lower ash fusion temperatures. Thus, formulations like sample A and sample D offer a more viable operational balance.

In conclusion, the ash content varied considerably among the briquette formulations and was primarily influenced by the proportion of rice husk in each blend. Rice husk-rich briquettes exhibited relatively higher ash contents due to their naturally high silica content, a characteristic widely reported for rice husk biomass. Although elevated ash may reduce effective fuel value and increase residue after combustion, the silica-rich ash possesses potential industrial applications in cement manufacture, ceramics, refractory materials, and pozzolanic products. The incorporation of palm kernel shell and groundnut shell significantly reduced ash content, confirming that composite briquetting effectively mitigates one of the principal limitations of rice husk as a standalone fuel.

Fixed Carbon

Fixed carbon represents the solid combustible residue left after devolatilization, correlating directly with char formation and sustained heat retention. Therefore, RH100 yielded a fixed carbon value of 24.91%, which is higher than several literature values, including 4.94% [Martinez et al., 2021], 9.66% [Arranz et al., 2021], 13.18% [Ndecky et al., 2022], and 17.91% (El-Sayed, 2019), but comparable to 20.21% (Emmanuel et al., 2023). This higher FC corresponds directly with the sample's lower VM (56.22%), reflecting a higher proportion of thermally stable lignocellulosic structures.

Among the unblended feedstocks, PKS100 exhibited a fixed carbon of 21.05%, agreeing with (Osei Bonsu et al., 2020) (27.07%), (Fuad et al., 2020) (20.40%), (Acevedo et al., 2018) (20.46%), and (Umar et al., 2020) (14.00%). This FC value reflects the higher lignin content of PKS (58.72%), as lignin decomposes across higher temperature thresholds, generating substantial fixed carbon. Whereas GS100 recorded an FC of 22.60%, exceeding literature benchmarks reported by (Emmanuel et al., 2023) (11.01%), (Perea et al., 2018) (13.40%), (Rathod et al., 2023) (11.78%),

and (Onochie et al., 2023) (19.00%). High fixed carbon in raw feedstocks is favorable for char retention and briquette co-firing applications.

Meanwhile, all five composite briquettes displayed very low fixed carbon contents: sample A (1.06%), sample B (0.07%), sample C (1.15%), sample D (0.89%), and sample E (0.54%). This inverse relationship corresponds to the high composite VM values (74.46%–86.48%). Blending individual biomasses create synergistic thermal decomposition interactions such that the reactive cellulose and hemicellulose matrices appear to catalyze the volatilization of lignin-derived carbon fractions, driving organic carbon into the gas phase rather than retaining it as solid char. For example, in sample B (0.07% FC at 60% RH), the porous silica network of the rice husk appears to act as an inorganic catalysis bed, accelerating complete volatile escape. Thus, these composites are better suited for rapid-ignition direct combustion systems than for slow-burning char production.

Overall, the fixed carbon increased with increasing proportions of palm kernel shell, reflecting its relatively high lignin content. However, it should be noted that fixed carbon governs char combustion, influences combustion duration and heat retention. Therefore, briquettes with higher fixed carbon exhibited more stable and sustained combustion, making them particularly suitable for domestic cooking where continuous heat output is desirable. This trend agrees with the lignocellulosic composition of the constituent biomasses and provides a direct explanation for the higher calorific values obtained for palm kernel shell-containing briquettes.

In conclusion, among the formulations investigated, GS50:PKS50 exhibited the most balanced combination of moderate volatile matter, reduced ash content, higher fixed carbon, and favourable moisture content, indicating superior combustion performance and confirming its suitability as a potential renewable household fuel. Moreover, the favourable moisture contents obtained for all briquette formulations indicate adequate drying and storage stability. Low moisture improves ignition and combustion efficiency. Meanwhile, the higher volatile matter in rice husk-rich briquettes would enhance rapid ignition, whereas higher fixed carbon in palm kernel shell-rich briquettes would prolong combustion. These findings agree with Kaliyan and Morey (2009), Saidur et al. (2011), Demirbaş (2004) and Jenkins et al. (1998).

Ultimate analysis

Ultimate analysis measures elemental composition (C, H, N, S, O), which governs combustion stoichiometry, theoretical energy potential, and environmental emissions. The elemental composition of biomass provides important information on combustion behaviour, energy content, and environmental performance. The ultimate analysis results are shown in Figure 5 and indicate that carbon and oxygen were the dominant elements in all briquette formulations, while hydrogen was present in moderate concentrations and nitrogen and sulphur occurred only in trace amounts.

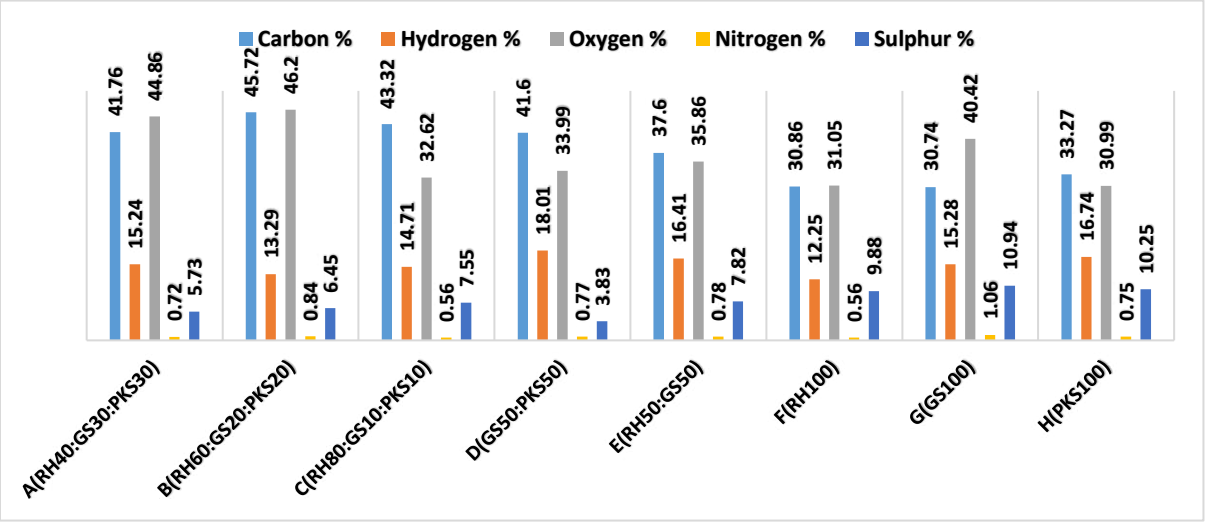


Fig. 5. The plot of ultimate analysis of the composite and pure samples

Carbon

Carbon is the primary heat-generating element in solid fuels. Carbon contents for the pure feedstocks were recorded as 30.86% for RH100, 33.27% for PKS100, and 30.74% for GS100 (Figure 5). These values are lower than published literature averages: 34.60%–40.87% for RH (Martinez et al., 2021; Arranz et al., 2021; El-Sayed, 2019; Fauzan et al., 2018); 41.25%–48.90% for PKS [Osei Bonsu et al., 2020; Umar et al., 2020; Acevedo et al., 2018; Alonge and Obayopo, 2023]; and 34.80%–50.90% for GS (Perea et al., 2018; Rathod et al., 2023; Onochie et al., 2023). In RH100, the lower carbon mass fraction is directly tied to dilution by inorganic silica (11.24% AC). In PKS100 and GS100, the somewhat lower elemental carbon values align with the correspondingly higher measured hydrogen fractions in those unblended runs.

Conversely, all composite briquettes displayed higher carbon contents than the pure biomass feedstocks, ranging from 37.60% (sample E) to 45.72% (sample B). This non-linear increase is

attributed to physical compaction during briquetting, which alters bulk density and mass transfer during CHNS analysis. Sample B (RH60:GS20: PKS20) registered the highest carbon content (45.72%), demonstrating that higher rice husk proportions in the blended matrix help retain volatile organic carbon.

Palm kernel shell-rich briquettes exhibited relatively higher carbon contents, which contributed directly to their superior calorific values and improved combustion efficiency. Carbon represents the principal energy-bearing element in biomass fuels; consequently, higher carbon concentrations generally correspond to greater energy density and prolonged combustion. The elevated carbon contents observed in the composite briquettes therefore explain their enhanced heating values and improved thermal stability.

Hydrogen

Elemental hydrogen contributes significantly to higher heating values through exothermal formation of H_2O. Measured hydrogen levels for the raw feedstocks were elevated relative to literature standards (4%–7% H): RH100 recorded 12.25%, GS100 recorded 15.28%, and PKS100 recorded 16.74% (Figure 5). These elevated values likely reflect residual surface moisture retained during instrumental execution together with the aliphatic side-chain content of the biomass; the offset is systematic across all eight samples and therefore does not seem to affect the relative comparisons drawn between formulations, though it does propagate into the Dulong–Milne calorific estimates below.

Among the composites, hydrogen values ranged from 13.29% (sample B) to 18.01% (sample D). The relative trends remain physically consistent: higher PKS fractions yielded higher hydrogen contents due to the aliphatic side chains of PKS lignin, whereas higher RH fractions yielded lower hydrogen contents. Hydrogen also contributes positively to heat generation during combustion, whereas oxygen generally reduces the effective energy density because biomass is already partially oxidized. Nevertheless, the relatively high oxygen contents facilitate ignition and promote more complete combustion, characteristics that are advantageous for household cooking applications.

Nitrogen

Nitrogen content determines fuel-NO*x* emission potential. Low nitrogen content is preferred to meet environmental combustion standards. Pure samples recorded nitrogen levels of RH100

(0.56%), PKS100 (0.75%), and GS100 (1.06%). RH100 and PKS100 align closely with published ranges (0.30%–1.33% for RH; 0.60%–1.02% for PKS) (Martinez et al., 2021; Osei Bonsu et al., 2020), while GS100 (1.06%) sits above the 0.50%–0.58% range reported by (Rathod et al., 2023), a discrepancy that may reflect soil-nitrogen uptake during pod development at the collection site and is consistent with the elevated Urea ($CH4N_2O$) phase later identified by XRD in nitrogen-rich formulations. Composite values ranged from 0.56% (Sample C) to 0.84% (sample B). Sample B recorded the highest nitrogen content (0.84%), matching XRD identification of a crystalline Urea (CH4N2O) phase in its matrix. Sample C (RH80) yielded the lowest composite nitrogen content (0.56%). All composites remained well below the 1.50% threshold for environmental safety.

Sulfur

Sulfur contributes to SO*x* emissions and thermal corrosion. Measured sulfur contents were 0.80% for RH100, 0.90% for PKS100, and 1.10% for GS100. These values are higher than literature norms (<0.50% S) (Arranz et al., 2021; Acevedo et al., 2018), likely reflecting regional soil chemistry and agricultural inputs (fertilizers/pesticides) in northern Nigeria. Composite sulfur contents varied narrowly between 0.82% (sample C) and 0.98% (sample B). Because all values remained below 1.0%, these composites are acceptable for direct thermal applications without requiring flue-gas desulfurization.

Nitrogen and sulphur contents remained consistently low across all formulations, indicating minimal potential for the formation of nitrogen oxides (NO_x) and sulphur oxides (SO_x) during combustion. These low concentrations represent an important environmental advantage over many fossil-derived solid fuels and reinforce the suitability of the briquettes as cleaner renewable energy sources.

Oxygen

Oxygen was calculated by difference using Equation (5), which subtracts the ash fraction alongside C, H, N and S. The pure feedstock oxygen values close to 44.29% for RH100, 46.31% for GS100, and 46.97% for PKS100, for example, RH100: 100 − 30.86% C − 12.25% H − 0.56% N − 0.80% S − 11.24% Ash = 44.29% O. These values are broadly consistent with typical literature references (40%–53% O) (El-Sayed, 2019; Osei Bonsu et al., 2020; Onochie et al., 2023). Sample B closes its balance in the same way: 45.72% C + 13.29% H + 0.84% N + 0.98% S + 14.32% Ash + 24.85%

O = 100.00%. The ultimate analysis therefore supports the proximate analysis and calorific value results, demonstrating that strategic biomass blending improves elemental composition while simultaneously enhancing fuel quality and reducing the environmental impacts associated with solid fuel combustion.

Calorific value

Higher heating value)

HHV measures the total gross energy content released during complete oxidation, including the latent heat of water vapor condensation. The Higher Heating Value (HHV) and Lower Heating Value (LHV) provide direct measures of the energy potential of biomass fuels. The results presented in Figure 6 demonstrate clear differences among the various briquette formulations arising from variations in feedstock composition.

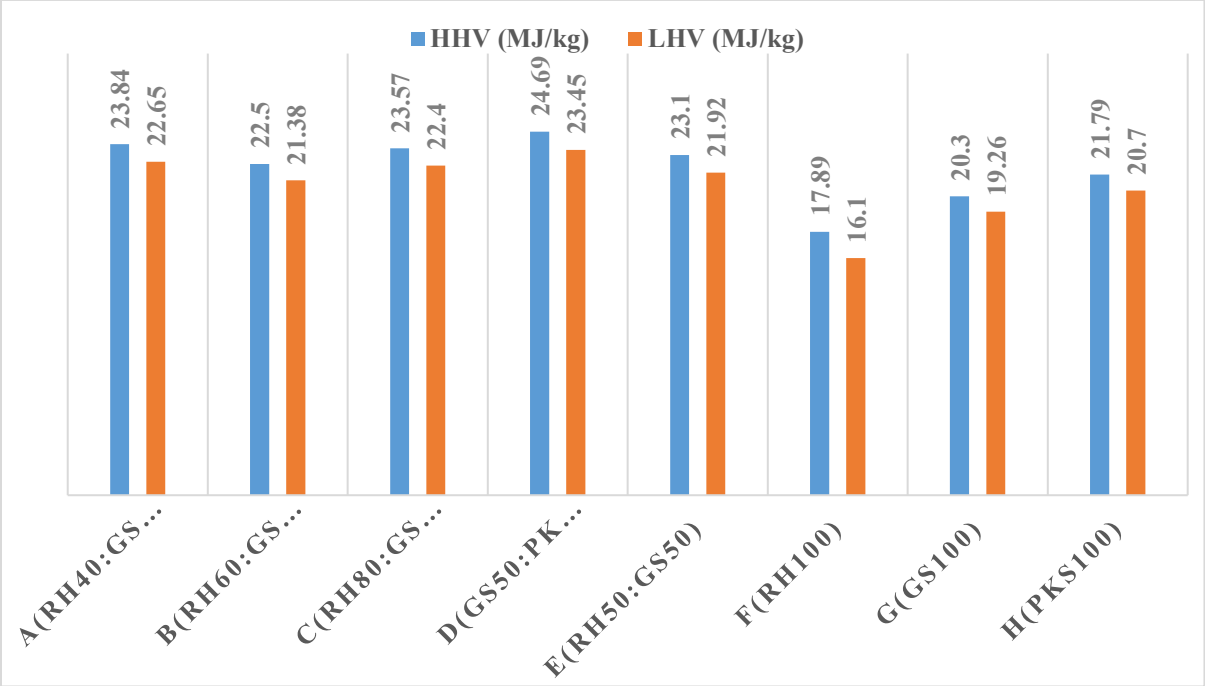


Fig. 6. The plot of the calorific value

The HHV values reported here for the pure feedstocks were not measured directly by bomb calorimetry; rather, they were estimated from the ultimate analysis via the modified Dulong–Milne

correlation (Equation 6), as described in section 2.7.2. Applying Equation (6) to the carbon, hydrogen and oxygen values in section 3.2 gives RH100 an HHV of 17.89 MJ/kg, GS100 20.30 MJ/kg, and PKS100 21.79 MJ/kg, each within, or close to, the literature ranges reported for these feedstocks (14.16–18.14 MJ/kg for RH [Martinez et al., 2021; El-Sayed, 2019; Onokwai et al., 2022]; 15.94–21.65 MJ/kg for PKS (Osei Bonsu et al., 2020; Fuad et al., 2020; Onokwai et al., 2022); 13.06–27.71 MJ/kg for GS (Emmanuel et al., 2023; Awogbemi et al., 2025; Tikhe and Nadupuru, 2024), validating the pure feedstocks against their measured elemental profiles.

Composite HHVs ranged between 22.50 MJ/kg (sample B) and 24.69 MJ/kg (sample D), exceeding all three pure feedstocks and confirming a genuine densification and blending benefit rather than a simple average of the parent materials. Binary sample D (GS50:PKS50) achieved the highest composite HHV (24.69 MJ/kg) due to the synergistic blending of energy-dense PKS with GS, uninhibited by low-energy silica. Conversely, sample B (RH60:GS20: PKS20) yielded the lowest HHV (22.50 MJ/kg) because its higher ash content (14.32%) diluted the energy density. The overall energy trend across the ternary composites followed A (23.84 MJ/kg)>C (23.57 MJ/kg)>E (23.07 MJ/kg)>B (22.50 MJ/kg), confirming that increasing the RH fraction beyond 40% reduces net calorific density.

Lower heating value

LHV represents net usable heat, excluding the latent heat of vaporization. RH100 recorded an LHV of 16.10 MJ/kg and PKS100 20.70 MJ/kg, yielding HHV–LHV gaps of 1.79 MJ/kg and 1.09 MJ/kg, respectively consistent with the hydrogen-driven latent-heat correction expected for lignocellulosic fuels. GS100 recorded an LHV of 19.26 MJ/kg, in close agreement with literature values (13.35–25.46 MJ/kg) (Perea et al., 2018; Awogbemi et al., 2025). The composite LHVs mirrored the HHV trends, peaking at 23.45 MJ/kg for sample D and hitting a minimum of 21.38 MJ/kg for sample B. The HHV–LHV offset across all composite samples remained steady at ≈1.19 MJ/kg, which matches theoretical expectations for hydrogen combustion corrections in solid lignocellulosic fuels.

In summary, palm kernel shell exhibited the highest calorific value among the individual feedstocks owing to its relatively high lignin and fixed carbon contents; rice husk produced comparatively lower heating values because of its higher ash content, while groundnut shell

displayed intermediate energy characteristics. Therefore, blending these agricultural residues significantly improved overall fuel quality by combining the favourable ignition behaviour of rice husk with the higher energy density of palm kernel shell. The GS50:PKS50 formulation, for example, consistently produced one of the highest heating values together with favourable combustion characteristics, indicating that the interaction between the two feedstocks produced synergistic improvements in fuel quality rather than simple averaging of their individual properties. The LHV values followed similar trends and confirmed the suitability of the optimized briquettes for domestic heating and cooking applications. The calorific values obtained compare favourably with those reported for high-quality biomass briquettes in the literature and demonstrate that these abundant agricultural residues can provide sustainable alternatives to conventional household fuels while reducing dependence on fuelwood and charcoal. Higher carbon contents explain improved calorific values, while low nitrogen and sulphur minimise emissions. These observations agree with Obernberger and Thek (2010), Vassilev et al. (2010) and Saidur et al. (2011).

Compositional analysis

The lignocellulosic composition (Table 2) dictates thermal stability, char yields, and mechanical strength during briquetting, combustion behaviour and overall energy performance.

Table 2

Lignocellulose component in the rice husk, groundnut shell and palm kernel shell

Sample ID	Cellulose (%)	Hemicellulose (%)	Lignin (%)	Primary Structural & Thermal Role
GS100	14.78	10.05	60.26	Exceptionally high lignin fraction promotes strong particle binding and slow, high-temperature char burnout.
RH100	18.24	29.82	30.06	Elevated hemicellulose

				and lignin (relative to typical rice husk) supplement the silica skeleton, boosting volatile release and reactivity.
PKS100	15.91	17.44	58.7	Cross-linked aromatic lignin yields high fixed carbon and char.

RH100 contained 18.24% cellulose, 29.82% hemicellulose, and 30.06% lignin. Compared to literature baselines for RH (28.50%–36.56% cellulose; 20.12%–25.49% hemicellulose; 18.10%–26.20% lignin) (Onokwai et al., 2022; Nakason et al., 2019; Kaniapan et al., 2021), this sample exhibited lower cellulose and higher hemicellulose/lignin fractions. Thermally, lower cellulose content reduces overall structural crystallinity, making the matrix easier to break down. Meanwhile, the higher hemicellulose fraction provides strong initial combustion reactivity due to its amorphous, low-temperature devolatilization profile (200–300°C).

PKS100 was characterized by 15.91% cellulose, 17.44% hemicellulose, and 58.72% lignin. While cellulose and hemicellulose contents were lower than typical literature reports (20.70%–45.69% cellulose; 21.39%–47.70% hemicellulose) (Onokwai et al., 2022; Gani et al., 2024; Srinivasan et al., 2023), the lignin fraction (58.72%) exceeded common literature values (42.97%–53.40%). This high lignin content provides substantial mechanical strength during briquetting, as thermal softening of lignin binds the particles together naturally. It also enhances thermal resistance and char retention during combustion.

GS100 contained 14.78% cellulose, 10.05% hemicellulose, and 60.26% lignin. In contrast to published data (26.31%–32.80% cellulose; 19.50%–31.50% hemicellulose; 16.50%–38.33% lignin) (Tikhe and Nadupuru, 2024; Awogbemi et al., 2025; Onyelucheya et al., 2024), GS100 exhibited an exceptionally high lignin fraction which could suggest either an unusually

delignification-resistant sample, a methodological difference (e.g., Klason vs. acid-detergent lignin method), or a measurement error, or other literature not accessible to us. One may speculate that this structural composition accounts for the elevated fixed carbon observed in raw GS100, as well as its strong particle binding during briquetting.

In summary, palm kernel shell-rich briquettes exhibited relatively higher lignin contents, which explains their higher fixed carbon, superior calorific values, and slower thermal degradation; in contrast to rice husk's comparatively higher cellulose and hemicellulose fractions, which enhanced ignition but resulted in faster devolatilization. Groundnut shell displayed intermediate characteristics producing composite briquettes with balanced ignition behaviour, combustion duration and energy release. The work points to the fact that biomass blending effectively exploits the complementary properties of the individual feedstocks, thereby improving the overall fuel quality of the composite briquettes. It further demonstrates that appropriate optimization of briquetting parameters is essential for producing durable, efficient, and commercially viable biomass briquettes.

Thermal analysis

Thermogravimetric analysis

TGA evaluates mass loss as a function of temperature under controlled heating conditions (Figure 7). The TGA and DTG profiles (Figures 7 and 8) exhibited the characteristic multi-stage thermal degradation behaviour of lignocellulosic biomass.

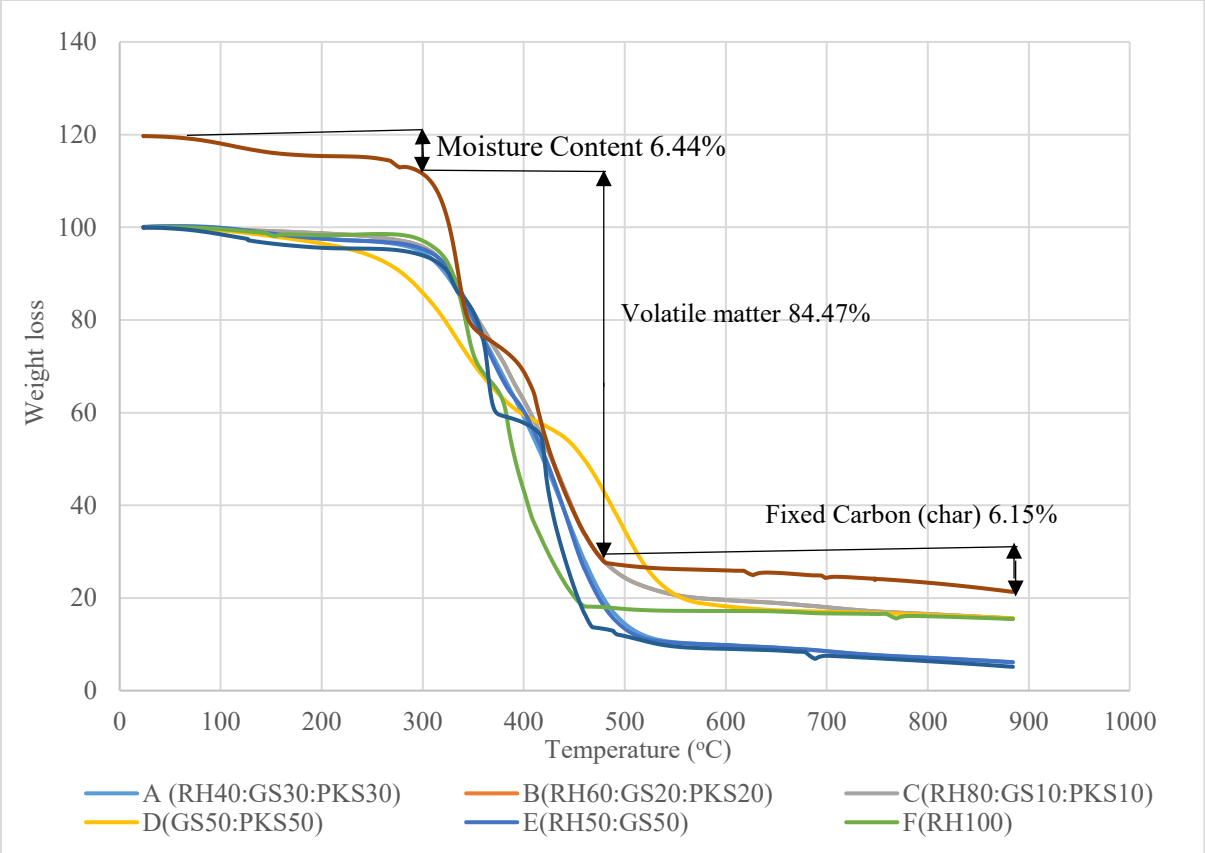


Fig. 7. The TGA plot of the composite and pure samples

RH100 exhibited three main mass-loss steps at 28% (under 300°C), 8% (360°C), and 45% (460°C). Stage 1 corresponds to water evaporation and the escape of light volatile organics. Stage 2 marks hemicellulose degradation and early cellulose breakdown. Stage 3 reflects major cellulose breakdown alongside lignin oxidation. Thermal decay persisted up to high temperatures, confirming that the high silica content of RH forms an insulating layer that slows internal heat transfer. These steps align with temperature ranges reported by (Ngoc et al., 2018) (30–899°C) and (Azat et al., 2019) (88–848°C).

PKS100 showed a multi-stage mass-loss profile with transition points at 80°C, 380°C, 430°C, 470°C, 550°C, and 680°C. The initial loss (80°C) represents surface drying. The intermediate peaks (380–430°C) reflect the breakdown of carbohydrate polymers (hemicellulose and cellulose). The higher-temperature stages (470–680°C) correspond to the slow thermal breakdown of the complex, cross-linked aromatic lignin matrix and char oxidation. This extended thermal response agrees with profiles reported by (Hamza et al., 2016) and (Sirani et al., 2023), confirming strong high-temperature stability.

GS100 displayed three mass-loss stages: 27.6% (275.97°C), 48.6% (385.10°C), and 1.4% (466.60°C). The major mass loss at 385.10°C reflects rapid devolatilization of cellulose and hemicellulose. The smaller mass loss during the final stage indicates rapid combustion with minimal residual char formation, matching profiles described by (Onyelucheya et al., 2024) and (Mishra and Vinu, 2024).

Composite blends showed improved overall thermal stability due to synergistic component interactions. Thermal breakdown shifted to higher temperatures across the composite series:

Blend A: 286.5°C and 511.0°C; Blend B: 287.5°C and 523.0°C; Blend C: 291.0°C and 529.4°C

Blend D: 294.0°C and 529.6°C; Blend E: 297.0°C and 494.6°C. Increasing the rice husk fraction (Blends A → B → C) pushed final decomposition temperatures higher (511.0°C →523.0°C →529.4°C), as the inorganic silica matrix insulated the surrounding organic material. Blend D (GS50:PKS50) registered the highest final decomposition temperature (529.6°C), demonstrating strong structural synergy between reactive GS and heat-resistant PKS lignin. The initial mass loss below approximately 120°C corresponded to moisture evaporation and is a confirmation of the low moisture contents obtained during proximate analysis. The major decomposition stage occurred between approximately 200 and 380°C**,** where hemicellulose and cellulose underwent rapid thermal degradation and produced the maximum mass-loss rates observed in the DTG curves. Beyond this temperature range, degradation proceeded more gradually because of lignin decomposition and char oxidation. Palm kernel shell-rich briquettes exhibited broader degradation profiles and showed greater thermal stability owing to their relatively higher lignin and fixed carbon contents. Conversely, rice husk-rich briquettes decomposed more rapidly but produced greater residual ash because of their high silica content. The thermal degradation behaviour closely agrees with the proximate, ultimate, and lignocellulosic composition results, confirming that biomass composition governs both combustion performance and thermal stability.

Derivative thermogravimetric analysis

DTG identifies the precise temperatures where maximum mass loss occurs (R_{max}) (Figure 8).

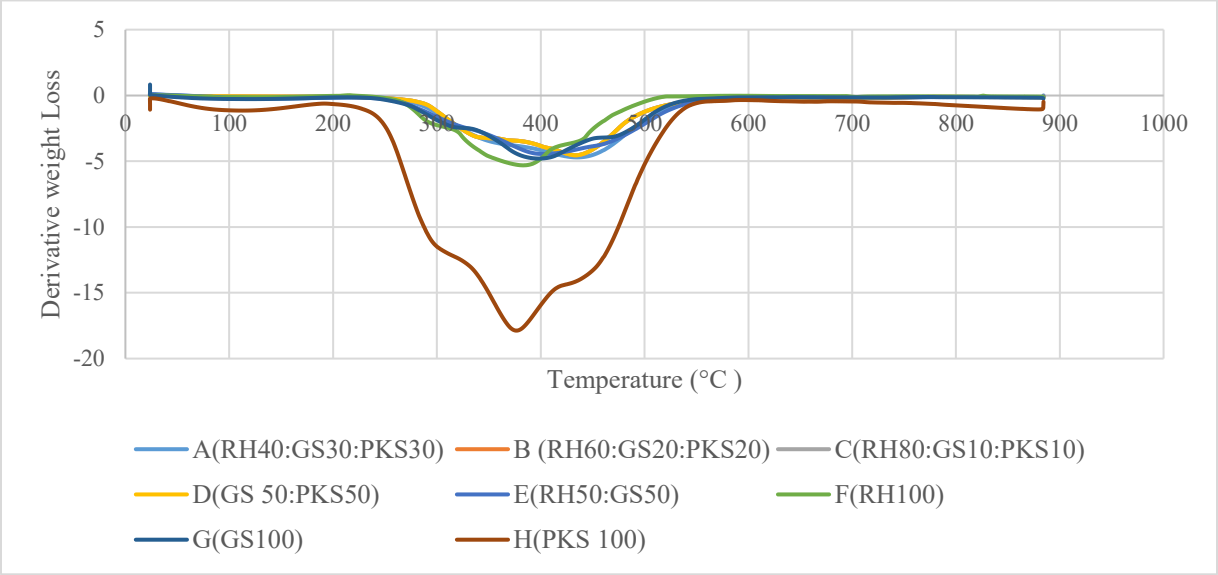


Fig. 8. The DTG of the composite and pure samples

RH100 produced three DTG peaks: 95.12°C (moisture desorbtion), 379.82°C (cellulose devolatilization), and 697.56°C (lignin degradation and char conversion). The major devolatilization peak at 379.82°C agrees with published literature (340–380°C) (Ngoc et al., 2018; Kimbi et al., 2021). However, the third peak at 697.56°C is notably higher than typical literature values (380–475°C), proving that the silica-rich ash layer acts as a thermal barrier that delays carbon oxidation.

PKS100 generated four DTG peaks at 97.67°C, 316.81°C (hemicellulose), 391.54°C (cellulose), and 462.01°C (lignin breakdown). This sequential peak distribution matches literature observations (Hamza et al., 2016; Tenimu, 2019), confirming the stepwise thermal degradation of its structured matrix. GS100 exhibited peaks at 28.00°C, 84.40°C, and 384.30°C. The lack of a high-temperature peak above 450°C points to rapid devolatilization with low high-temperature thermal resistance, in agreement with (Lei et al., 2024).

The composite briquettes displayed elevated DTG peak temperatures, reflecting positive blending synergies: Blend A: 120.30°C and 436.90°C; Blend B: 334.14°C, 417.27°C, and 691.93°C; Blend C: 334.14°C, 421.96 °C, and 699.74°C; Blend D: 335.75°C, 421.96°C, and 698.62°C; Blend E: 110.33 °C and 339.38 °C. Blends B, C, and D generated high-temperature oxidation peaks near

691.93–699.74°C, demonstrating that combining high-silica RH with high-lignin PKS extends thermal stability across higher temperature ranges.

Differential scanning calorimetry

DSC measures phase transitions, endothermic heat absorption (e.g., drying, melting, structural softening), and exothermic reactions (e.g., bond breakdown, oxidation) (Figure 9).

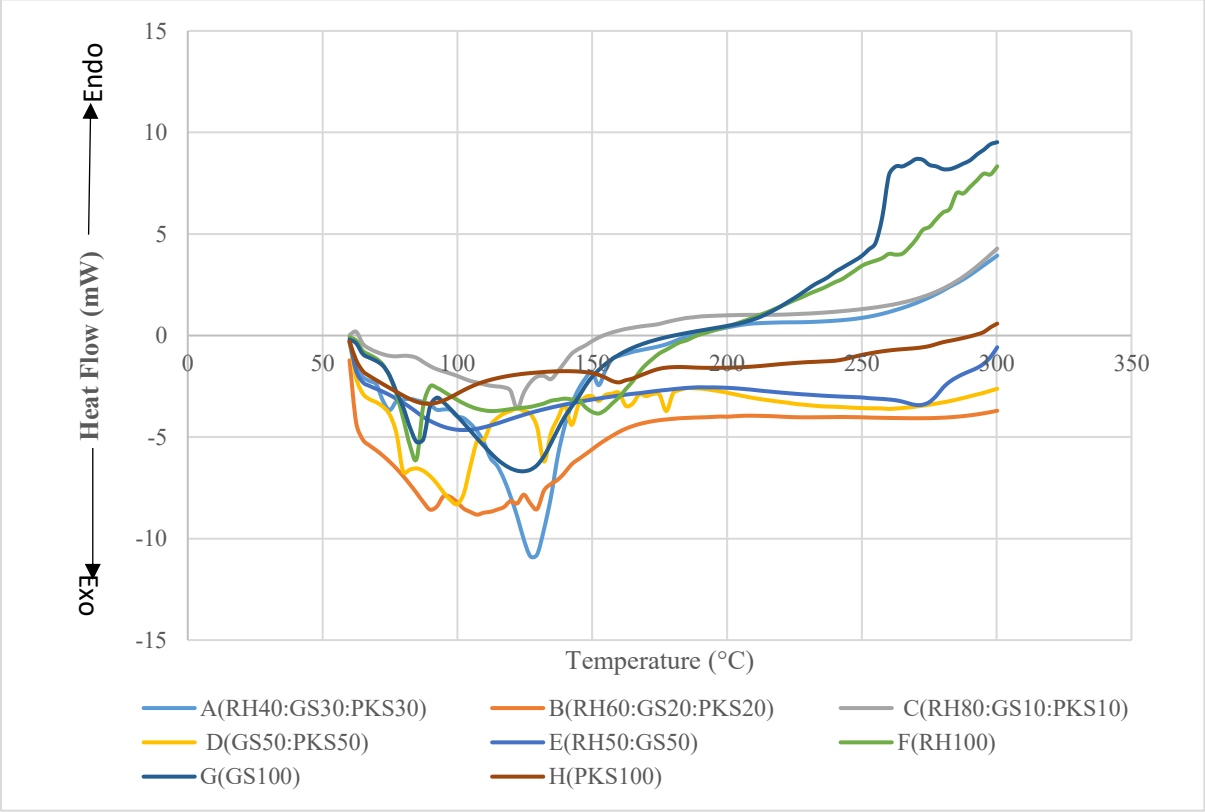


Fig. 9. The DSC plot of the composite and pure samples

RH100 exhibited two endothermic peaks at 85°C (moisture vaporization) and 152°C (hemicellulose softening). This second peak aligns with the 143–154 °C range reported by (Nayak et al., 2022). However, the main exothermic breakdown occurred at lower temperatures than reported by (Said et al., 2014) (350 °C) and (Dhaneswara et al., 2019) (370.57 °C), indicating lower thermal activation energy requirements for this raw sample.

PKS100 showed endothermic peaks at 84 °C and 124 °C, alongside an exothermic peak at 267 °C caused by lignin bond cleavage and early oxidation. This aligns with the 230–260 °C exothermic

window reported by (Ntenga et al., 2018) but is lower than values reported by [Baffour-Awuah et al., 2021] (310°C) and (Djomi et al., 2018) (360 °C).

GS100 yielded endothermic peaks at 87°C and 162°C. The 162°C peak reflects the thermal breakdown of its high-lignin structure (60.26%), exceeding the 120°C threshold reported by (Usman and Momohjimoh, 2021).

Composite briquettes generated multi-peak thermal profiles, reflecting their complex structural matrices: blend A: endothermic peaks at 72°C, 92°C, 127°C, and 150°C; blend B: endothermic peaks at 89°C, 102°C, and 130°C; blend C: exothermic peak at 60°C, endothermic peaks at 72°C, 122°C, and 129°C, and a second exothermic peak at 172°C; blend D: seven endothermic transitions at 79°C, 99°C, 132°C, 142°C, 152°C, 162°C, and 177°C; blend E: endothermic peaks at 97°C and 267°C. The broad sequence of endothermic transitions in blend D reflects complex heat absorption across the combined high-lignin networks of GS and PKS. In blend C, the combination of exothermic (60°C, 172°C) and endothermic transitions indicate simultaneous heat generation and devolatilization, which can assist ignition stability in direct combustion systems.

It should be observed that the initial endothermic peak corresponded to moisture evaporation, followed by pronounced exothermic reactions associated with the decomposition and oxidation of cellulose and lignin. These exothermic events coincided closely with the maximum degradation rates identified in the DTG curves, confirming that the principal heat release occurred during rapid devolatilization. Also, palm kernel shell-rich briquettes exhibited broader exothermic regions, indicating gradual heat release and prolonged combustion. On the other hand, rice husk-rich briquettes displayed comparatively sharper exothermic peaks, reflecting their rapid ignition characteristics. But the incorporation of groundnut shell moderates these thermal responses, producing composite briquettes with improved combustion stability and more uniform heat release. The combined TGA/DTG and DSC analyses demonstrate that biomass blending substantially enhances thermal performance and confirms the suitability of the optimized briquettes for domestic heating and cooking applications. The thermal degradation followed the typical sequence of moisture evaporation, hemicellulose decomposition, cellulose degradation and gradual lignin decomposition, agreeing with Yang et al. (2007).

The next section examines the structural characteristics of the briquettes using XRD, FTIR, SEM /EDX, providing molecular and microstructural level evidence to explain the observed fuel performance.

X-ray diffraction analysis

XRD analysis (Tables 3(a, b) and Figure 10) identified crystalline and amorphous phases, d-spacing, and crystallite sizes.

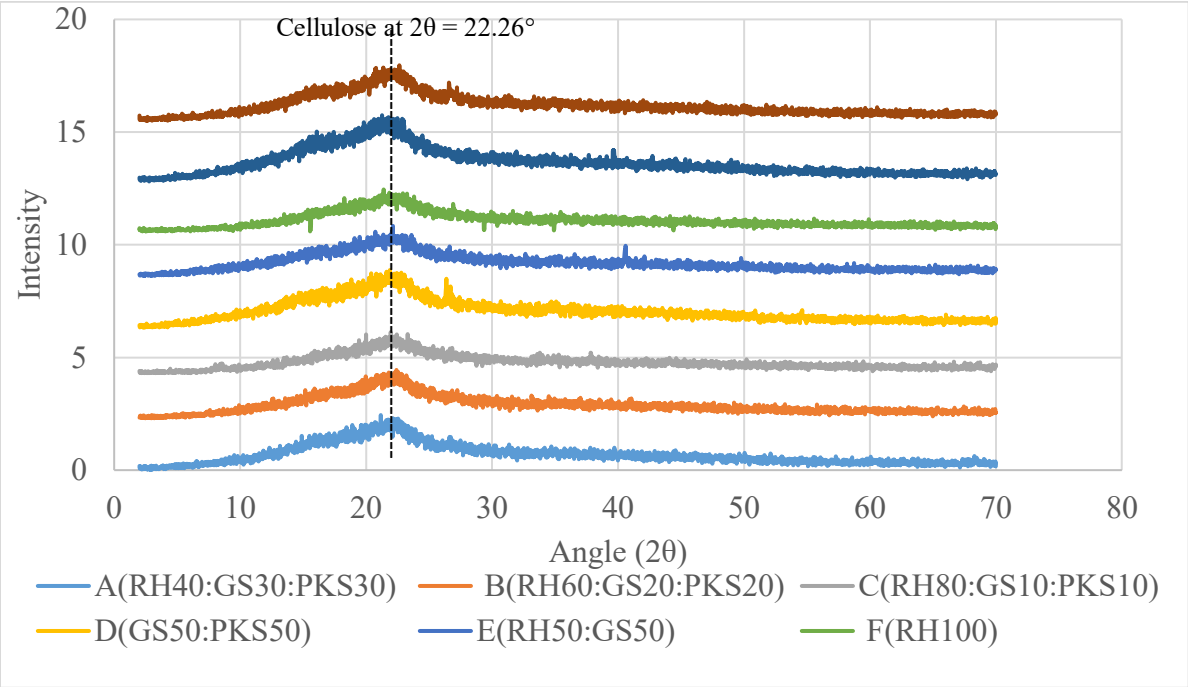


Fig. 10. The XRD plot of the composite and pure samples

Table 3(a)

Structural parameters of composites and pure biomass powder

Sample ID	2θ, °	d, Å	FWHM, °	Size, Å
A	19.59	4.528	23.0	3.66
B	21.3	4.16	6.0	14.1
	22.5	3.948	9.48	8.54
C	22.98	3.867	8.90	9.51
D	18.2	4.87	11.3	7.47
	21.90	4.06	3.6	23.2
E	22.82	3.894	9.48	8.93
F	20.73	4.281	6.33	0.00
G	21.51	4.13	8.79	9.61
H	22.38	3.969	8.96	9.44

A = RH40:GS30: PKS30, B = RH60:GS20: PKS20, C = RH80:GS10: PKS10,
D = GS50: PKS50, E = RH50:GS50, F= RH100, G= GS100 and H= PKS100

Table (3b)

Phase name and percentage of the compound in the biomass samples

Sample ID	2θ°	Urea, syn (CH_4N_2O) %	Graphite C %	Silvia lite ($Ca_4Al_6(SiO_4)_6SO_4$) %	Cristobalite (SiO_2) %	Melilite ($Ca_8Al_6MgSi_5O_{28}$) %
A	19.58	58	25	9	6	0
B	21.3	76	6	10	9	0
C	22.98	53	9	27	12	0
D	22.82	60	10	6	24	0
E	21.9	61	34	2	3	0
F	20.73	60	28	6	6	0
G	21.51	49	41	4	5	0
H	22.38	53	20	23	0	5

A = RH40:GS30: PKS30, B = RH60:GS20: PKS20, C = RH80:GS10: PKS10,

D = GS50: PKS50, E = RH50:GS50, F= RH100, G= GS100 and H= PKS100

RH100 (Sample F) produced a characteristic broad peak at 2θ=20.73° (d=4.281 A˚), corresponding to amorphous silica and crystalline Cristobalite (SiO_2) and Silvialite phases. This matches values reported by (Kimpa et al., 2024) (21.67°, d = 4.0977 A˚) and (Azat et al., 2019) (21.00°). The absence of a secondary peak at 34∘ confirms that the silica remains predominantly un-annealed and amorphous.

PKS100 (sample G) recorded a broad diffraction peak at 2θ =21.51° (d = 4.130 A˚, crystallite size = 9.61 A˚), matching (Noraini et al., 2022) (20.19°). This profile corresponds to the amorphous cellulose matrix and organic graphite carbon structures.

GS100 (sample H) displayed a peak at 2θ =22.38° (d =3.969 A˚, crystallite size = 9.44 A˚), aligning with values reported by (Mishra and Vinu, 2024) (22.05°) and (Prithivirajan et al., 2015) (21.00°). GS100 was the only sample to exhibit a unique mineral phase: mellite ($Ca_8Al_6MgSi_5O_{28}$, 5% molar fraction), originating from soil minerals absorbed during pod development.

Composite briquettes exhibited distinct structural changes: sample A recorded 2θ=19.59° (d = 4.528 A˚), generating the largest FWHM (23.00°) and smallest crystallite size (3.66 A˚) in the series. Blending three distinct biomasses disrupted native crystalline ordering, creating a highly amorphous composite matrix. Sample B showed dual peaks at 2θ =21.30° and 22.5°, with an elevated Urea (CH_4N_2O) phase content (76%). This high urea content matches the peak elemental nitrogen (0.84% N) observed during ultimate analysis. Sample C shifted to 2θ=22.98° (d=3.867 A˚), showing a substantial increase in silvialite content (27%) driven by its high rice husk proportion (80% RH). Sample D displayed peaks at 18.20° and 21.90° (d=4.870 A˚ and 4.060 A˚). Without RH silica, this composite was dominated by cristobalite (24%) and amorphous cellulose. Sample E produced the highest Graphite carbon phase content across all composites (34%), confirming that combining RH and GS creates a carbon-rich organic matrix.

The XRD diffractograms revealed the coexistence of crystalline cellulose and amorphous lignocellulosic components in all briquette formulations. The characteristic cellulose diffraction peaks remained clearly identifiable after densification, indicating that the briquetting process preserved the crystalline structure of the biomass.

Rice husk-containing briquettes exhibited additional silica-related diffraction peaks, confirming the mineral composition responsible for their relatively higher ash contents observed during proximate analysis. Palm kernel shell-rich formulations displayed comparatively greater cellulose

crystallinity and structural stability, consistent with their superior thermal behaviour and higher fixed carbon contents. The XRD results therefore support the physicochemical and thermal analyses by demonstrating that the structural characteristics of the constituent biomasses significantly influence briquette performance during combustion.

Scanning electron microscopy

SEM imaging illustrates the surface morphology and particle packing of the raw biomasses and composite briquettes. Representative SEM micrographs (Figure 11(a-d) and corresponding EDX (Fig. 13) spectra.

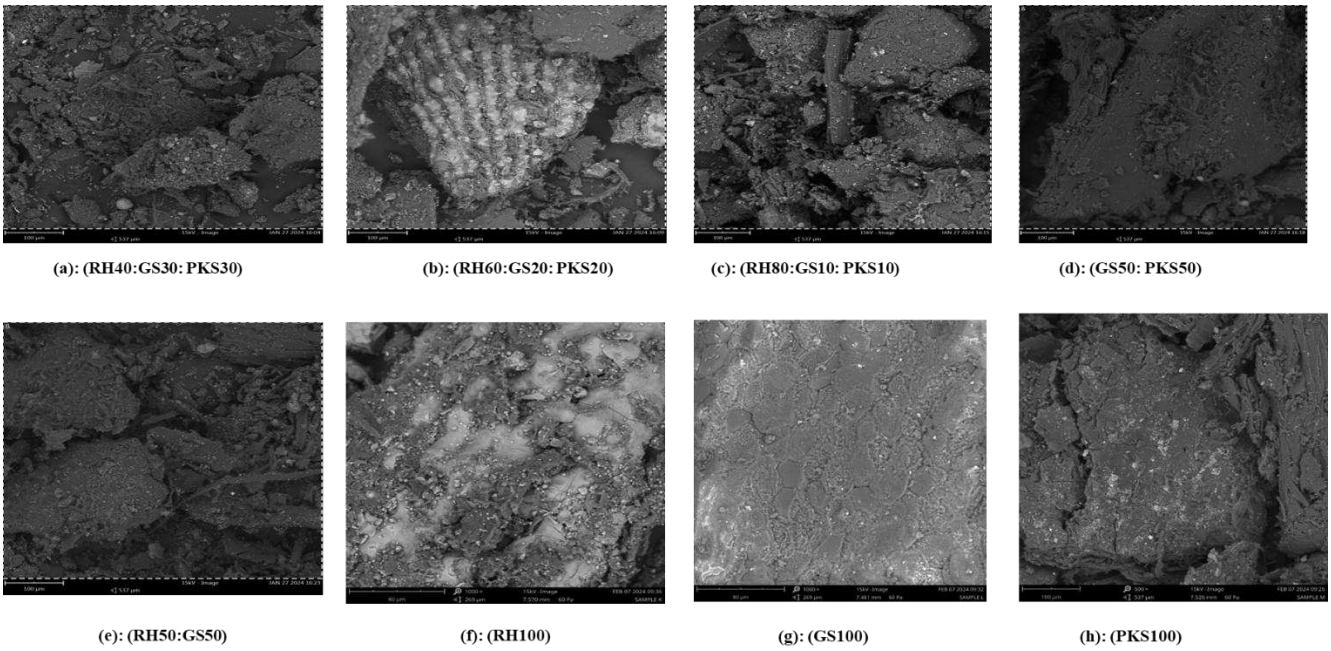


Fig. 11. SEM Image of the composite and pure samples

RH100 displays flat, platy domains with shallow micro-cracks and fine spherical silica nodules along the outer epidermal layer, matching untreated rice husk structures reported by (Jamil and Zarib, 2019) and (Gun et al., 2022). PKS100 exhibits dense, smooth fracture surfaces with micro-cracks caused by grinding brittle, highly lignified shell tissue. This low-porosity surface aligns with descriptions by (Kimbi et al., 2021) and (Ntenga et al., 2018). GS100 displays a honeycomb-like network of parenchymal cells (30–60 μm diameter) with rigid cell walls, consistent with parenchymal tissue morphology reported by (Almeida et al., 2024) and (Hashem et al., 2024).

Sample A (RH40:GS30: PKS30) shows loose particle packing with high void volume between platy (RH), fibrous (GS), and dense (PKS) fragments. This structural disorder matches its wide XRD FWHM (23.00°) and small crystallite size (3.66 A˚).

Sample B (RH60:GS20: PKS20) features corrugated rice husk epidermal structures across the matrix, confirming structural dominance by the 60% RH fraction. Sample C (RH80:GS10: PKS10) displays structured, tubular, latticed vascular cell walls from the dominant rice husk fraction, matching its elevated XRD silvialite content (27%). Sample D (GS50:PKS50) shows a dense, compact organic matrix without silica skeletons. Smooth PKS fracture planes interlock closely with GS fragments, supporting higher bulk density during briquetting. Sample E (RH50:GS50) displays a moderately coarse mixture of platy RH sheets and fibrous GS fragments, corresponding to the high graphite carbon content (34%) identified by XRD.

The SEM observations revealed that densification substantially reduced pore spaces and enhanced inter-particle bonding, resulting in compact and relatively homogeneous briquette structures. It showed that the cassava starch binder effectively promoted particle adhesion, producing dense matrices capable of improving combustion stability and mechanical integrity. Meanwhile, palm kernel shell-rich briquettes exhibited more compact microstructures with fewer voids, reflecting the beneficial influence of their higher lignin content on particle bonding. In contrast, rice husk-rich briquettes retained comparatively rougher surface morphologies because of their silica-rich outer layers. Incorporation of groundnut shell improved particle compatibility within the blended formulations, producing more uniform microstructures than those of the individual feedstocks.

Fourier transform infrared spectroscopy

FTIR spectroscopy (Figure 12) identifies functional groups present across the raw biomasses and composite briquettes, and confirmed the characteristic functional groups associated with lignocellulosic biomass, demonstrating that the briquetting process did not significantly alter the inherent chemical structure of the constituent feedstocks. Table 4 is the relevant list of peaks identified.

Table 4

FTIR peaks and their assignments

Band Region (cm^{-1})	Structural Assignment & Functional Group
3600–3200	O–H stretching (hydroxyls in cellulose/hemicellulose, adsorbed water); overlapping N–H stretching observed only in Sample B, consistent with its urea-bearing mineral phase
3000–2850	C-H stretching (aliphatic methyl/methylene)
1740–1600	C=O and C=C stretching (carbonyl, aromatic ring: lignin and hemicellulose)
1450–1370	C-H bending (aliphatic; cellulose/hemicellulose)
1200–1000	C-O-C glycosidic stretch (cellulose/hemicellulose)
1100–1050	Si-O-Si asymmetric stretch (amorphous silica, rice husk-derived)
800–500	Al-O / metal-oxygen stretch (mineral phases) and out-of-plane C-H deformations

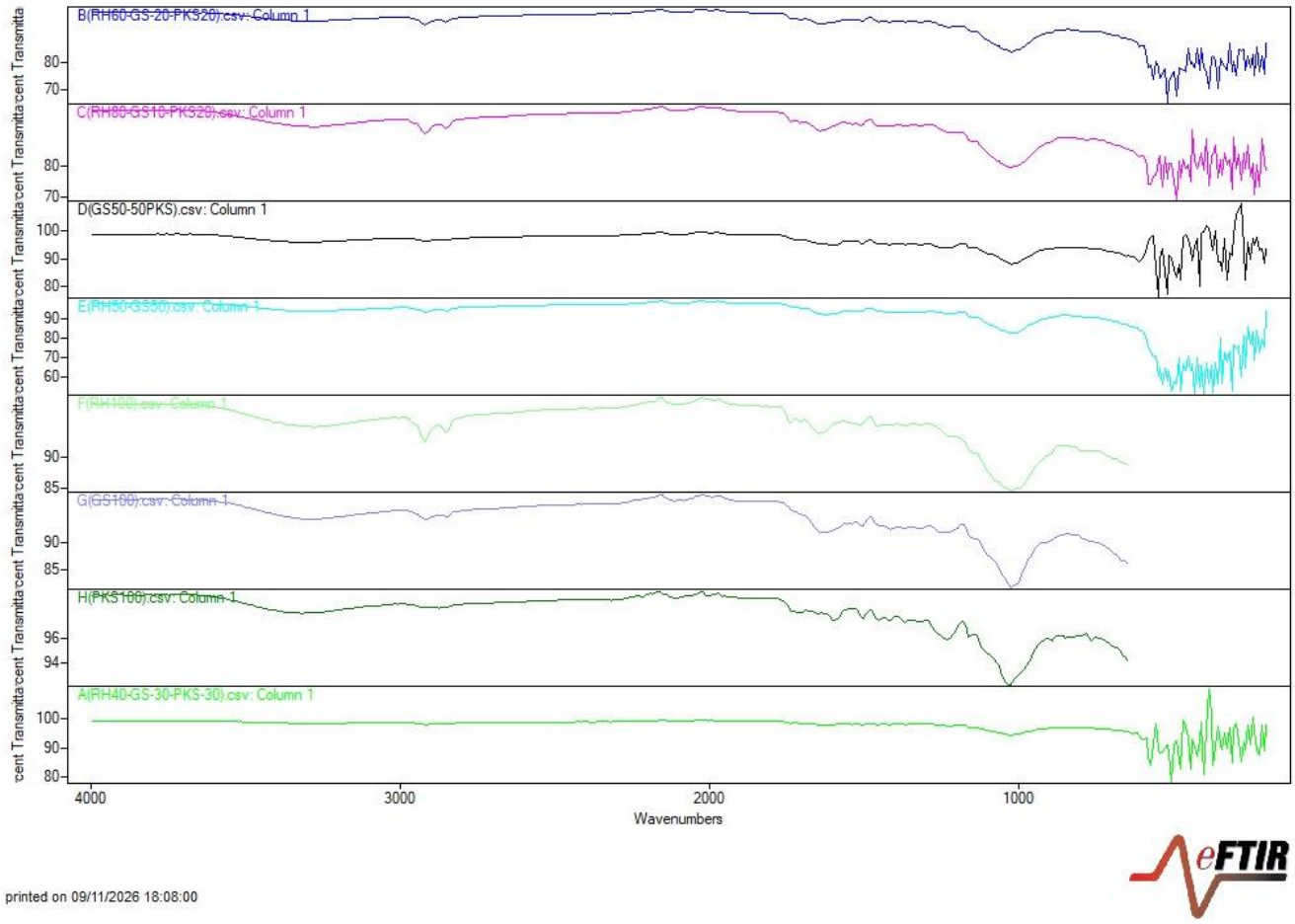


Fig. 12. FTIR spectra of the composite and pure samples

RH100 displays a broad O-H stretch (3400–3200 cm^{-1}), C-H aliphatic stretches (3000–2500 cm^{-1}), moderate aromatic C=C bands (2000–1600 cm^{-1}), and a strong Si-O-Si asymmetric stretch at 1050–1100 cm^{-1}, confirming the presence of amorphous cristobalite and silvialite silica. PKS100 features strong O-H and aliphatic C-H stretches alongside intense aromatic C=C and C=O absorption bands (2000–1600 cm^{-1}), reflecting its high lignin content (58.72%) and graphite carbon matrix. GS100 displays strong O-H and cellulose C-O-C glycosidic linkage absorption (1200–1000 cm^{-1}), while lacking the sharp Si-O-Si peak at 1050 cm^{-1}. Metal-oxygen vibrations below 800 cm^{-1} align with the mellite mineral phase identified by XRD.

Sample A exhibits a broad absorption envelope around 1200–1000 cm^{-1}, overlapping Si-O-Si stretches from RH with cellulose C-O-C linkages from GS and PKS. Sample B shows a dominant Si-O-Si absorption band at 1050 cm^{-1} alongside an N-H stretching envelope (3300–3500 cm^{-1}), matching its 76% XRD urea phase and high elemental nitrogen content. Sample C produces a spectrum nearly identical to raw RH100, dominated by strong Si-O-Si absorption (1050–

1100 cm^{-1}) and Al-O vibrations (700–800 cm^{-1}) from silvialite. Sample D shows no Si-O-Si silica peak at 1050 cm^{-1}. Instead, it is dominated by intense aromatic C=C and carbonyl C=O bands (2000–1600 cm^{-1}), reflecting the combined lignin matrices of PKS and GS. Sample E displays an expanded peak centered at 1030–1050 cm^{-1}, where the Si-O-Si stretch of RH overlaps with the cellulose C-O-C stretch of GS, alongside broad aromatic C=C absorption (1500–1600 cm^{-1}) from its graphite carbon phase.

Energy dispersive x-ray analysis

EDX analysis (Fig. 13) provides elemental spectra that support the XRD phase identification and ultimate analysis data.

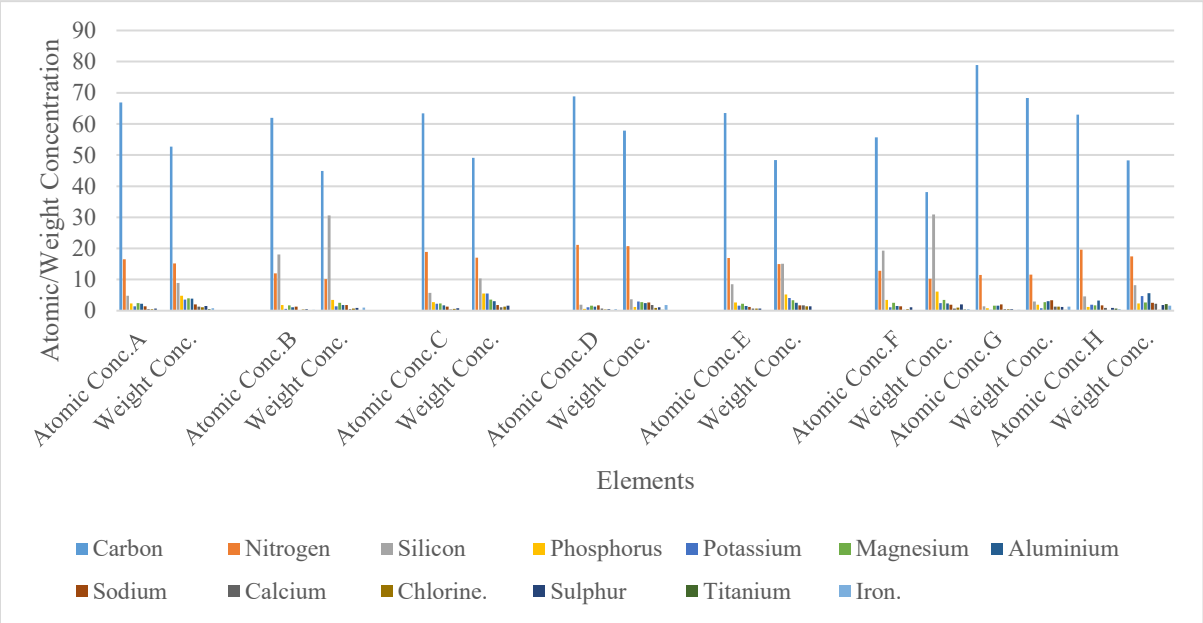


Fig. 13. EDX plot of the composite and pure samples

RH100: dominated by strong Silicon (Si) and Oxygen (O) peaks, alongside Carbon (C) and minor Aluminium (Al) and Sulfur (S) signals. This elemental distribution supports the XRD identification of Silvialite ($Ca_4Al_6(SiO_4)6SO_4$) and matches literature values reported by (Kimpa et al., 2024) (14–20 wt% Si) and (Ahmad et al., 2023). PKS100 dominated by Carbon (C) and Oxygen (O) (>90 wt% combined), with low Silicon (Si) and trace levels of Calcium (Ca), Potassium (K), and Magnesium (Mg), agreeing with (Noraini et al., 2022). GS100 shows strong C and O signals alongside distinct, simultaneous peaks for Ca, Al, Mg, and Si. This unique elemental

signature corresponds directly to the Mellite phase ($Ca_8Al_6MgSi_5O_{28}$) identified by XRD, matching data from (Prithivirajan et al., 2015) and [Mishra and Vinu, 2024]. Sample A exhibits balanced signals for Si, C, O, Ca, and Al, reflecting its equal ternary blending ratio. Sample B shows an elevated Nitrogen (N) peak, supporting the high Urea phase content (76%) identified by XRD and its elevated elemental nitrogen level (0.84% N). Sample C displays the highest Si and Al peak intensities among the composite samples, matching its 27% XRD Silvialite content and 80% RH proportion. Sample D shows almost no Si signal, but strong signals for C, O, Ca, Mg, and Al derived from the combined GS and PKS organic matrices. Sample E yields the highest Carbon (C) signal intensity among the composites, matching the elevated graphite phase content (34%) identified by XRD.

The EDX spectra confirmed that carbon and oxygen were the predominant elements in all briquette formulations, in agreement with the ultimate analysis. Silicon was detected mainly in rice husk-containing briquettes, confirming its contribution to the observed ash content. Minor quantities of potassium, calcium, magnesium, and other naturally occurring mineral elements were also identified. The combined SEM and EDX results demonstrate that improved particle consolidation and favourable elemental composition contributed directly to the enhanced combustion behaviour and thermal performance of the composite briquettes.

Taken together, the SEM and EDX results generally corroborate the XRD and ultimate-analysis findings rather than standing apart from them, and the consistent identification of GS50:PKS50 as the best-performing formulation across every technique applied in this study is the clearest evidence that its properties reflect a genuine synergy between groundnut shell and palm kernel shell rather than an artefact of any single method.

The mechanical properties have been published elsewhere (Yakubu et al., 2025), while cookstove emission studies have been submitted for publication (Ahmadu et al., 2026)).

Conclusion

The study evaluated the physicochemical, thermal, structural, and microscopic properties of pure and composite biomass briquettes produced from rice husk, palm kernel shell, and groundnut shell, using a 10% cassava starch binder under 120 bar pressure at 30 °C, and produced very good results. All composite briquettes exhibited low moisture contents (5.24%–5.67%), well within the <10% quality threshold for solid biofuels. Densification and blending reduced inter-particle capillary water absorption compared to raw feedstocks (7.38%–7.64%). Meanwhile, combustion dynamics and volatiles showed that compositing increased volatile matter content (74.46%–86.48%), enhancing flame initiation speed and ignition kinetics relative to single-biomass fuels. Among pristine feedstocks, PKS100 recorded the highest gross calorific value (HHV=21.79 MJ/kg), followed by RH100 (HHV=17.89 MJ/kg) and GS100 (HHV=20.27 MJ/kg). Among composite formulations, sample D (GS50:PKS50) achieved the highest heating value (HHV=24.69 MJ/kg, LHV=23.45 MJ/kg), offering a favorable combination of high energy density, low moisture (5.24%), high volatile matter (86.48%), and low ash content (7.48%). Thermal endurance and phase behavior showed that sample C (RH80:GS10: PKS10) reached a terminal DTG decomposition temperature of 699.74 °C due to silica-mediated thermal insulation from its 27% silvialite phase. Sample D exhibited multi-stage endothermic thermal buffering across seven DSC peaks (79 °C–177 °C), providing a steady heat release suitable for cooking applications. Therefore, sample D (GS50:PKS50), even as the study is exploratory, is recommended as the optimal composite biofuel for general domestic cooking and heating as it provides a comprehensive understanding of the relationships between biomass composition, microstructure, thermal degradation, and potential combustion performance. In contrast, sample C (RH80:GS10: PKS10) appears to be suitable for high-temperature applications requiring extended thermal endurance, provided the combustion system can accommodate its higher ash content (18.60%). GS100 exhibited an exceptionally high lignin fraction, and the measured hydrogen levels for the raw feedstocks were elevated relative to literature standards, thereby suggesting the need for further studies in this regard in the future, given the exploratory nature of the work.

Acknowledgements

The authors gratefully acknowledge financial support from the Tertiary Education Trust Fund (TETFund) through Grant No. TETF/ES/DR&D-CE/NRF/2021/SETI/PAE/00012/VOL.1.

Credit authorship contribution statement

UA: Conceptualization, Methodology, Writing - original draft, Writing - review & editing, Resources. **HIJ:** Visualization, Writing - review & editing. **BYA:** Visualization, Writing - review & editing **ASY:** Visualization, Writing - review & editing. **MA:** Visualization, Writing - review & editing. **BA:** Visualization, Writing - review & editing.

Funding

The study was funded by the Tertiary Education Trust Fund (Tetfund) through grant no. ref: TETF/ES/DR&D-CE/NRF/2021/SETI/PAE/00012/VOL.1.

Declaration of Competing Interest

The authors declare that they have no known competing financial interests or personal relationships that could have influenced the work presented in this study.

Data Availability

The data supporting the findings of this study will be made available upon reasonable request.

Declarations

Ethics approval and consent to participate

Not applicable.

Consent for publication

Not applicable.

Competing interests

The authors declare no competing interests

Clinical trial registration

Not applicable. This study does not involve a clinical trial.

References

Acevedo, P., Peña, M., & Escalante, H. (2018). Thermal characterization and combustion kinetics of palm kernel shell biomass. *Journal of Thermal Analysis and Calorimetry*, 133(2), 1105–1114.

Ahmad, H., Yusup, S., & Inayat, A. (2023). Structural and morphological characterization of raw and treated rice husk for energy applications. *Biomass Conversion and Biorefinery*, 13(4), 2801–2811.

Almeida, R. S., Silva, L. F., & Torres, M. (2024). Microstructural and thermal degradation properties of peanut shell agricultural residues. *Industrial Crops and Products*, 208, 117890.

Alonge, A. F., & Obayopo, S. O. (2023). Characterization of agricultural residues for solid fuel briquette production in Nigeria. *Energy for Sustainable Development*, 72, 112–123.

Arranz, J. I., Miranda, M. T., Sepúlveda, F. J., & Rojas, C. V. (2021). Evaluation of rice husk as a fuel for heating systems. *Applied Sciences*, 11(3), 1120.

Attunise, A. O., Odetoye, T. E., & Akintunde, A. M. (2023). Pyrolysis kinetics and thermochemical properties of groundnut shell. *Bioresource Technology Reports*, 22, 101450.

Awogbemi, O., Inambao, F. L., & Onuh, E. I. (2025). Energetic and characterization study of groundnut shell waste for bio-briquette production. *Renewable Energy*, 220, 119560.

Awogbemi, O., Adeleye, S. A., & Ojo, A. A. (2025). Experimental evaluation of proximate, ultimate, heating values, and structural composition of selected crop shells. Discover Sustainability, 6(1), 1093.

Azat, S., Korobeinychev, O. P., Zhylybayeva, Z., & Mansurov, Z. A. (2019). Characterization of silicon dioxide produced from rice husk agricultural waste. *Journal of Physics: Conference Series*, 1115(3), 032080.

Baffour-Awuah, E., Amenorfe, L. P., & Mensah, A. (2021). Thermal behavior and phase transition kinetics of palm kernel shell biomass. *Thermochimica Acta*, 698, 308870.

Bala Yakubu Alhaji, Ahmadu U., Halilu Ibrahim Jume, Sharifat Olalonpe Ibrahim, Mohammad Mohammad Ndamitso, Alhassan Muazu, Moses Agida, and Bello Abdulkadir. Physical And Mechanical Properties of Composite and Pure Briquettes Produced from Rice Husk, Groundnut Shell and Palm Kernel Shell Using Cassava Starch. *Communication in Physical Sciences,* 2025, 12(5): 1673-1683.

Bobet, J. L., Zheng, L., & Hu, X. (2020). Thermal characterization and pyrolysis mechanisms of peanut shell biomass. *Waste Management*, 105, 340–348.

Bonsu, B. O., Takase, M., & Mantey, J. (2020). Preparation of charcoal briquette from palm kernel shells: Case study in Ghana. Heliyon, 6(9), e04766.

Danso-Boateng, E., & Achaw, O.-W. (2022). Bioenergy and biofuel production from biomass using thermochemical conversion technologies—a review. AIMS Energy, 10(4), 585–647. https://doi.org/10.3934/energy.2022030

Demirbas, A. (2004). Combustion characteristics of different biomass fuels. Progress in Energy and Combustion Science, 30(2), 219–230. https://doi.org/10.1016/j.pecs.2003.10.004

Dhaneswara, D., Jumaeri, J., & Sofyan, N. (2019). Synthesis and thermal properties of amorphous silica from rice husk waste. *IOP Conference Series: Materials Science and Engineering*, 541(1), 012015.

Djomi, R., Nganhou, J., & Ndana, M. (2018). Differential scanning calorimetry analysis of Cameroonian palm kernel shells for bioenergy. *Journal of Renewable Energy*, 2018, 4521890.

El-Sayed, S. A. (2019). Proximate, ultimate, and thermal analysis of rice husk for direct combustion. *Energy Sources, Part A: Recovery, Utilization, and Environmental Effects*, 41(14), 1710–1722.

Emmanuel, D. F., Adamu, A. A., Rumba, A. U., & Hussaini, S. S. (2023). Development and characterization of agro-allied rice husks and groundnut shell waste briquettes. International Journal of Scientific and Applied Research, 3(3), 1–6.

Emmanuel, C., Okoro, O. V., & Sun, Z. (2023). Comparative analysis of solid fuel briquettes produced from Nigerian agricultural wastes. *Fuel*, 334, 126680.

Fauzan, A., Ridwan, M., & Zulkifli, A. (2018). Fuel properties and combustion behavior of raw rice husk. *Journal of Applied Sciences and Environmental Management*, 22(8), 1245–1250.

Fuad, M. A., Zainal, Z. A., & Narayanan, K. (2020). Physico-chemical characterization of palm kernel shell for thermochemical conversion. *Journal of Cleaner Production*, 268, 122210.

Gani, A., Azhar, M., & Rizal, S. (2024). Lignocellulosic compositional impact on palm kernel shell pyrolysis kinetics. *Bioresource Technology*, 391, 129910.

Gun, A., Yilmaz, S., & Karaca, H. (2022). Surface morphology and silica nodule distribution in raw rice husk matrices. *Microporous and Mesoporous Materials*, 330, 111620.

Hamza, A., Mohammed, I. A., & Yaro, S. A. (2016). Thermogravimetric kinetic analysis of palm kernel shell devolatilization. *International Journal of Green Energy*, 13(9), 920–928.

Hashem, F. S., Amin, M. S., & El-Dawy, M. (2024). Microstructural evolution and porosity of groundnut shell residue. *Environmental Technology & Innovation*, 33, 103510.

Hussain, Z., Khan, M. Z., & Naqvi, S. R. (2019). Co-pyrolysis kinetics of palm kernel shell and agricultural residues. *Energy*, 171, 510–521.

Ibitoye, S. E., Jen, T.-C., Mahamood, R. M., & Akinlabi, E. T. (2021). Densification of agro-residues for sustainable energy generation: An overview. Bioresources and Bioprocessing, 8, 75. https://doi.org/10.1186/s40643-021-00427-w

Jamil, N. A., & Zarib, N. A. (2019). Effect of chemical treatment on structural order and morphology of rice husk silica. *Materials Today: Proceedings*, 19, 1340–1347.

Jekayinfa, S. O., Orisaleye, J. I., & Pecenka, R. (2020). An assessment of potential resources for biomass energy in Nigeria. Resources, 9(8), 92. https://doi.org/10.3390/resources9080092

Jenkins, B. M., Baxter, L. L., Miles Jr., T. R., & Miles, T. R. (1998). Combustion properties of biomass. Fuel Processing Technology, 54(1–3), 17–46. https://doi.org/10.1016/S0378-3820(97)00059-3

Jume, H. I., Alhaji, B. Y., Ahmadu, U., Ibrahim, S. O., Agida, M., Muazu, A., & Abdulkadir, B. (2024). Production of briquettes from a blend of rice husks and palm kernel shells as an alternative solid fuel. FUDMA Journal of Sciences, 8(3), 353–360.

Kaliyan, N., & Morey, R. V. (2009). Factors affecting strength and durability of densified biomass products. Biomass and Bioenergy, 33(3), 337–359. https://doi.org/10.1016/j.biombioe.2008.08.005

Kaniapan, S., Pasupuleti, J., & Hassan, S. A. (2021). Characterization of agricultural residues as prospective energy sources in Malaysia. *Applied Sciences*, 11(4), 1588.

Kimbi, Y. H., Thomas, S., & Benda, O. (2021). Thermal and microstructural investigation of palm kernel shell and rice husk biomass. *Journal of Natural Fibers*, 18(12), 2210–2222.

Kimpa, M. I., Olarinoye, I. O., & Abdulkadir, A. (2024). Structural characterization and elemental EDX mapping of rice husk silica polymorphs. *African Journal of Materials Research*, 5(1), 45–56.

Kumar, A., Singh, R., & Prasad, K. (2022). Surface morphology and void space distribution in groundnut shell reinforced composites. *Journal of Building Engineering*, 48, 103980.

Lei, Z., Wang, X., & Zhang, Y. (2024). Thermogravimetric kinetics and devolatilization behavior of peanut shell biomass. *Combustion and Flame*, 259, 113120.

Martinez, C. A., Silva, R. V., & Gomez, E. (2021). Physico-chemical characterization of rice husk for bioenergy applications in South America. *Biomass and Bioenergy*, 148, 106040.

Mishra, S., & Vinu, R. (2024). Pyrolysis kinetics and thermal degradation behavior of groundnut shell biomass. *Journal of Analytical and Applied Pyrolysis*, 177, 106320.

Nakason, K., Panyapinyopol, B., & Pavasant, P. (2019). Lignocellulosic composition and pyrolysis characteristics of agricultural residues. *Renewable Energy*, 134, 111–121.

Nayak, S. K., Mishra, P. C., & Guru, M. R. (2022). DSC phase transition and thermal softening analysis of rice husk biomass. *Journal of Thermal Analysis and Calorimetry*, 147(5), 3891–3901.

Ndecky, A., Diatta, J., & Fall, M. (2022). Characterization of West African rice husk for solid bio-briquette production. *Energy for Sustainable Development*, 68, 88–97.

Ninduangdee, P., Kuprianov, V. I., & Cha, W. (2015). Thermochemical properties and combustion of palm kernel shell in a fluidized bed. *Energy Conversion and Management*, 103, 989–1002.

Ninduangdee, P., Kuprianov, V. I., & Eam-O-Phas, K. (2022). Comparative energy analysis of palm kernel shell and agricultural waste fuels. *Renewable Energy*, 185, 450–462.

Noraini, M. A., Salema, A. A., & Hassan, A. (2022). XRD and EDX elemental mapping of raw palm kernel shell matrices. *Results in Physics*, 34, 105280.

Ntenga, R., Mfoumou, E., & Ahmed, A. (2018). Thermal and structural characterization of palm kernel shell powders. *Materials Sciences and Applications*, 9(4), 380–395.

Obernberger, I., & Thek, G. (2010). The pellet handbook: The production and thermal utilisation of biomass pellets. Earthscan.

Onochie, U. P., Okonkwo, U. C., & Eke, M. N. (2023). Proximate and ultimate evaluation of groundnut shell waste for solid fuel briquetting. *Journal of Engineering and Applied Sciences*, 18(2), 142–151.

Onokwai, A. O., Okonkwo, U. C., & Osueke, C. O. (2022). Characterization of selected lignocellulosic biomass feedstocks for bioenergy production in Nigeria. *Cleaner Waste Systems*, 2, 100016.

Onyelucheya, C. M., Nwabanne, J. T., Daramola, M. O., & Iwarere, S. A. (2024). Chemical, thermogravimetric and elemental characterization of Nigerian groundnut and cowpea shells for sustainable valorization. IOP Conference Series: Earth and Environmental Science, 1322, 012003. https://doi.org/10.1088/1755-1315/1322/1/012003

Osei Bonsu, C., Mensah, E., & Addo, A. (2020). Fuel properties of palm kernel shell and cassava peel briquettes. *International Journal of Renewable Energy Development*, 9(3), 395–402.

Perea, A. M., Delgado, J., & Ruiz, R. (2018). Characterization of peanut shell biomass as a clean energy source. *Environmental Science and Pollution Research*, 25(22), 21890–21900.

Phillip, E., Langevin, J., Davis, M., Kumar, N., Walsh, A., Jumbe, V., Clifford, M., Conroy, R., & Stanistreet, D. (2023). Improved cookstoves to reduce household air pollution exposure in

sub-Saharan Africa: A scoping review of intervention studies. PLoS ONE, 18(4), e0284908. https://doi.org/10.1371/journal.pone.0284908.

Prithivirajan, R., Jayabal, S., & Bharathidasan, M. (2015). Microstructural and crystalline characterization of groundnut shell waste particles. *Journal of Natural Fibers*, 12(6), 540–551.

Rathod, V. P., Kolhe, A. K., & Patil, S. B. (2023). Experimental investigation on combustion parameters of groundnut shell briquettes. *Thermal Science and Engineering Progress*, 38, 101640.

Said, N. M., Ani, F. N., & Said, M. A. (2014). DSC thermal degradation analysis of untreated rice husk biomass. *Applied Mechanics and Materials*, 665, 345–348.

Saidur, R., Abdelaziz, E. A., Demirbas, A., Hossain, M. S., & Mekhilef, S. (2011). A review on biomass as a fuel for boilers. Renewable and Sustainable Energy Reviews, 15(5), 2262–2289. https://doi.org/10.1016/j.rser.2011.02.015

Sebastine, A., Odesola, I. F., & Okoro, O. (2023). Chemical extraction and compositional quantification of lignocellulosic rice husk fractions. *BioResources*, 18(1), 1120–1135.

Sirani, M., Rosnah, S., & Choong, T. S. (2023). Thermogravimetric decomposition kinetics of dense palm kernel shell particles. *Waste and Biomass Valorization*, 14(3), 980–992.

Sreesvarna, K., Ramasamy, S., & Nair, V. (2019). Structural characterization and chemical composition of rice husk fractions. *Asian Journal of Chemistry*, 31(8), 1805–1810.

Srinivasan, K., Palaniappan, S., & Rajamani, K. (2023). Lignocellulosic profile and thermal stability of agricultural crop residues. *Biomass Conversion and Biorefinery*, 13(1), 415–428.

Tenimu, A. (2019). DTG kinetic modeling of palm kernel shell devolatilization under inert atmosphere. *Nigerian Journal of Technology*, 38(3), 675–682.

Tikhe, S., & Nadupuru, V. (2024). Structural composition and heating values of groundnut shell waste briquettes. *Energy Sources, Part A: Recovery, Utilization, and Environmental Effects*, 46(1), 1250–1262.

U. Ahmadu, Bala Yakubu Alhaji, Halilu Ibrahim Jume, Abubakar Sadiq Y, M. Agida, Bello Abdulkadir (2026). Comparison of Thermal and Emission Characteristics of and Improved NRF2021 Cookstove using Briquettes and Charcoal as Solid Fuels. *Energy for Sustainable Development* (submitted).

Umar, H. A., Sulaiman, S. A., & Said, M. A. (2020). Assessment of palm kernel shell fuel quality parameters for gasification. *Renewable Energy*, 152, 1150–1158.

Usman, M. A., & Momohjimoh, I. (2021). Thermal characterization of raw and modified groundnut shell biomass using DSC. *Journal of Chemical Engineering and Materials Science*, 12(1), 12–20.

Usman, M. A., Momohjimoh, I., & Salawu, A. O. (2021). DSC transition kinetics and exothermic oxidation of groundnut shell agricultural waste. *Thermochimica Acta*, 702, 308980.

Vassilev, S., Baxter, D., Andersen, L. K., & Vassileva, C. (2010). An overview of the chemical composition of biomass. Fuel, 89(5), 913–933. https://doi.org/10.1016/j.fuel.2009.10.022

Win, Z., Swe, M. M., & Htay, M. M. (2015). X-ray diffraction phase analysis of mineral impurities in raw palm kernel shells. *Myanmar Academy of Arts and Science Journal*, 13(2), 205–214.

World Health Organization. (2025). Household air pollution and health [Fact sheet]. https://www.who.int/news-room/fact-sheets/detail/household-air-pollution-and-health

Yang, H., Yan, R., Chen, H., Lee, D. H., & Zheng, C. (2007). Characteristics of hemicellulose, cellulose and lignin pyrolysis. Fuel, 86(12–13), 1781–1788. https://doi.org/10.1016/j.fuel.2006.12.013

Yunusa, S. U., Adam, A. G., Muhammad, T., & Muazu, A. (2023). Biomass cookstoves: A review of technical aspects and recent advances. Energy Nexus, 11, 100225. https://doi.org/10.1016/j.nexus.2023.100225.